ÇUKUROVA UNIVERSITY
INSTITUTE OF NATURAL AND APPLIED SCIENCES

MSc THESIS

Hamed KAGHAZCHI

DETERMINATION OF DIAMETER DISTRIBUTION OF NERVE FIBERS FROM COMPOUND ACTION POTENTIAL DATA

DEPARTMENT OF ELECTRICAL AND ELECTRONICS ENGINEERING

ADANA, 2012

ÇUKUROVA UNIVERSITY
INSTITUTE OF NATURAL AND APPLIED SCIENCES

DETERMINATION OF DIAMETER DISTRIBUTION OF NERVE FIBERS FROM COMPOUND ACTION POTENTIAL DATA

Hamed KAGHAZCHI

MSc THESIS

DEPARTMENT OF ELECTRICAL AND ELECTRONICS ENGINEERING

We certify that the thesis titled above was reviewed and approved for the award of degree of the Master of Science by the board of jury on 04/01/2013

…….....	……...	…….....
Asst. Prof. Dr. M. Kerem ÜN	Assoc. Prof. Dr. Ulus ÇEVİK	Assoc. Prof. Dr. Zekeriya TÜFEKCİ
SUPERVISOR	MEMBER	MEMBER

This MSc Thesis is written at the Department of Institute of Natural And Applied Sciences of Çukurova University.
Registration Number:

Prof. Dr. Selahattin SERİN
Director
Institute of Natural and Applied Sciences

ÖZ

YÜKSEK LİSANS TEZİ

SİNİR LİFLERİNİN ÇAP DAĞILIMININ BİLEŞİK AKSİYON POTANSİYELİ VERİLERİ YARDIMIYLA BELİRLENMESİ

Hamed KAGHAZCHI

ÇUKUROVA ÜNİVERSİTESİ
FEN BİLİMLERİ ENSTİTÜSÜ
ELEKTRİK ELEKTRONİK MÜHENDİSLİĞİ ANABİLİM DALI

Danışman :Yrd. Doç. Dr. M. Kerem ÜN
Yıl: 2013, Sayfa: 59
Jüri :Yrd. Doç. Dr. M. Kerem ÜN
:Doç. Dr. Ulus ÇEVİK
:Doç. Dr. Zekeriya TÜFEKCİ

Ana sinirler çok sayıda sinir fiberlerinden oluşur. Sinirde bir sinyal oluştuğunda, bu sinyal her fiber boyunca ayrı ayrı, bir aksiyon potansiyeli şeklinde (tek fiber aksiyon potansiyeli (SFAP)) iletilir. İletim hızı fiberin çapına ve miyelin tabakası ile kaplı olup olmamasına bağlıdır.

SFAP'ler, süperpoze olarak, klinik çalışmalarda sıkcana ölçülen bir büyüklük olan bileşke aksiyon potansiyelini (CAP) oluştururlar. CAP'in profili ve iletim hızı, bu CAP'i oluşturan SFAP'lerin iletim hızıyla yakından ilgilidir. Yaralanmalar veya ilaç kullanımı sonrasında, CAP profilinde değişiklik olabilir. Bu patolojilerin hangi fiberlere hasar verdiğini ve SFAP'yi nasıl değiştirdiğini anlamak, teşhis ve tedavi açısından önemlidir.

Sinirlerdeki fiberlerlerin sayısı bazen binlerle ifade edilir. Bu bakımdan, fiberlerin yarı çaplarının ve SFAP'lerin hızlarının, analitik bir fonksiyon yardımıyla ifade edilebilen sürekli bir dağılıma sahip olduğu varsayılabilir. Eldeki bir CAP için, bu CAP'i verecek çap dağılımını bulmak için (varsayılan fonksiyonun türüne bağlı olarak lineer veya nonlineer olabilen) bir gradyan optimizasyonu yöntemi uyguladık. Parametreleri optimizasyon ile, çap dağılımına en yakın eğriyi verecek şekilde belirlenen farklı fonksiyonları (özellikle Gauss dağılımı eğrisini ve polinomları) inceledik. 8.derece polinomun, biyolojik olarak mevcut hemen hemen tüm dağılımları tarif ettiğini gözlemledik.

Anahtar Kelimeler: CAP, fiber çap dağılımı, sayısal optimizasyon, SFAP

ABSTRACT

MSc THESIS

DETERMINATION OF DIAMETER DISTRIBUTION OF NERVE FIBERS FROM COMPOUND ACTION POTENTIAL DATA

Hamed KAGHAZCHI

ÇUKUROVA UNIVERSITY
INSTITUTE OF NATURAL AND APPLIED SCIENCES
DEPARTMENT OF ELECTRICAL AND ELECTRONICS ENGINEERING

Supervisor :Asst. Prof. Dr. M. Kerem ÜN
Year: 2013, Pages: 59
Jury :Asst. Prof. Dr. M. Kerem ÜN
:Assoc. Prof. Dr. Ulus ÇEVİK
:Assoc. Prof. Dr. Zekeriya TÜFEKCİ

Major nerves are made of large numbers of nerve fibers. When a signal is initiated in the nerve, it is transmitted along each fiber via an action potential (called single fiber action potential (SFAP)) which travels with a velocity that is related with the diameter of the fiber and whether the fiber is covered with a myelin sheath or not. The additive superposition of SFAP's constitutes the compound action potential (CAP) of the nerve, a quantity that is often measured in clinical neurophysiology. The shape of the CAP and its traveling pattern is closely related with velocity distribution of the SFAP's forming the CAP. After injuries or usage of certain drugs, the CAP profile of the nerve might change. It is important to understand which fibers are damaged/deactivated by these pathologies for diagnostic and therapeutic purposes.

The number of fibers in a nerve can be measured sometimes in thousands. Hence, it is possible to assume a continuous distribution for the fiber diameters and the velocities of SFAP can be represented by an analytical function. For a given CAP, we have applied a (depending on the function type, linear or nonlinear) gradient optimization technique to determine the diameter distribution that will result to this CAP. We have assumed different types of functions, in particular polynomials and Gaussian distributions, whose parameters are found through optimization to give the best fit to the actual diameter distribution function. We have observed that an 8^{th} order polynomial can capture almost all fiber distributions present in vivo.

Key Words: CAP, fiber diameter distribution, numerical optimization, SFAP

ACKNOWLEDGMENTS

I would like to thank my supervisor, Asst. Prof .Dr. M. Kerem ÜN for his endless support, encouragement and great supervision. It has been a great honor to have Mr. Kerem ÜN as my supervisor.

I would like to thank my committee members Assoc. Prof. Dr. Ulus ÇEVİK and Assoc. Prof. Dr. Zekeriya TÜFEKCİ for their valuable input and suggestions.

I want to express my appreciations to Rouhollah DIZBARI for his advice and shared experiences.

Special thanks go out to my uncle Mr. Mostafa KAGHAZCHI, who has always given me support and help during my studies.

Finally, I would like to thank my family; my father, my mother and my brother HADI for their unconditional love.

CONTENTS **PAGE**

LSIT OF FIGURES **PAGE**

LIST OF ABBREVIATONS

CAP : Compound action potential

CVD : Conduction velocity distribution

SFAP : Single fiber action potential

FDD : Fiber diameter distribution

CAPE : Experimental compound action potential

Amp : Amplifier

$H(\phi)$: Fiber diameter distribution function

M : Number of fiber classes

A : Amplitude

E : Error

$\mathbf{J(x)}$: Jacobian matrix

V : Transmembrane potential

R_m : Passive membrane resistance

I_{pp} : Applied current

I_s : Transmembrane current

R : Gas constant

F : Faraday constant

T : Absolute temperature

C_m : Membrane capacitance

f(t) : SFAP waveform function

nf : Total number of fibers

k : Dielectric constant for the insulator

l : Distance between stimulation and recording electrodes

r : Channel resistance

g : Membrane conductance

d : Thickness of insulator

v_i : Propagation velocity

w_i : Weighting coefficients

τ_1 : rising phase rate

τ_2 : total duration of a SFAP

τ_m : Time constant

ε_0 : Permittivity of free space

λ : Space constant

ϕ : Fiber diameter

1. INTRODUCTION

1.1. Prologue

In the nervous system, nerves are typically made of an abundant number of nerve fibers. The electrical signal that travels along a nerve fiber is called a *single fiber action potential* (SFAP). The combined electrical activity of the nerve fibers is termed as *compound action potential* (CAP) of the nerve. CAP recorded from a nerve bundle contains information concerning the number of active fibers and the propagation velocities of their action potentials. CAP is affected by different factors such as drugs, disease and injury. As a result, for the functional investigation of nerves in situ, the CAP has widespread application in basic research and, in particular, for the assessment of neuromuscular disease (Rubinstein and Sharger 1990), (Wells and Gazoni 1999), (Dalkilic and Pehlivan 2002). An analysis of the CAP can reveal the population size of active fibers, the distribution of their diameters and in case of injury or disease; it can be used to estimate the level of damage in the fiber population. Hence, many clinical branches, such as neurology, orthopedics, and physical medicine, rely in part on the electrophysiological properties of nerves for characterizing the peripheral nerve function in health and disease.

A proper analysis of CAP is clinically important to determine the level of abnormality in the nerve and requires certain mathematical tools to be utilized.

1.2. Compound action potential and nerve-fiber diameter distribution

According to Hirose et al, the continuous CAP can be described as the convolution of single fiber action potentials (SFAP) waveform and the latency distribution, and in the discrete time the CAP can be expressed as the circular convolution of the delay sequence and the sampled SFAP (Gu, Gander and Chrichlow 1996).

Myelin is a special insulating lipid layers that covers certain nerve fibers. As a result, nerve fibers can grossly be classified as either myelinated or nonmyelinated.

The conduction velocity of a healthy myelinated fiber is proportional to the axon diameter and generally is much higher than that of a nonmyelinated fiber. Action potential travels in each fiber with a potentially different velocity. CAP can be considered as the combination of these action potentials and contains implicit information about conduction velocity distribution (CVD) in the fibers. Consequently, the fiber diameter distribution in the nerve can also be deduced using the known relationships between the fiber diameter and propagation velocity. Since only healthy fibers respond to electrical excitation, diameter distribution of healthy nerve fiber can be estimated from sampled CAP signals, recorded by means of surface electrodes. That way, neuromuscular disease, injury and regeneration can be diagnosed more quantitatively and non-invasively (Papadopoulou and Panas 1999). Direct measurement of nerve-fiber diameter is possible only by biopsy or similar invasive interventions (Pollak and Wan 1997).

The myelin sheath, which is closely related to the propagation velocity, is highly sensitive to internal environment variations. As a result, measurement of CVD has also been added to diagnostic tests of several metabolic disorders such as diabetes mellitus (Harati 1987), uremic syndrome, and other toxic syndromes (Seneviratne and Deiris 1970), (Wichman, et al. 1985), which are known to alter the myelin sheath resulting in decreased nerve CV (Gonzalez-Cueto and Parker 2002).

1.3. Objective and Thesis Layout

In numerical model simulations, the fiber distribution is commonly characterized by a histogram of propagation velocity or fiber diameter. In other words, the fibers diameter values are rounded to the nearest integer and the fibers are categorized into a finite number of groups according to this value. Clearly, this simplification brings a certain error into the calculations. In reality, the fiber diameter is a continuous quantity. A typical nerve contains a relatively high number of fibers (Schonhoven and Stegeman 1991) that it is possible to describe the diameter distribution using a continuous distribution function rather than a discrete histogram. Assuming a continuous fiber distribution allows (linear or nonlinear) optimization to

be used in order to find the correct distribution using experimental data. Yet, this approach seems to be totally ignored in the literature.

The objective of this thesis is to evaluate the continuous approach for the determination of the fiber distribution in nerves.

Chapter 2 gives a brief outline of the physiology of the nervous system for understanding of its anatomy and functioning. Some basic concepts of bioelectricity is also presented here.

The physiology of action potentials is described in detail in Chapter 3. The forward and inverse problems of CAP are introduced and the related existing literature about CAP modeling is reviewed in this chapter.

Chapter 4 describes the proposed continuous function approach to CAP modeling. The determination of the fiber distribution leads to linear and nonlinear optimization problems, which are also explained in detail in this chapter.

The results of the example problems are presented in Chapter 5.

A thorough evaluation of the results and the related discussion, along with future research directions are given in Chapter 6.

2. BIOLOGY AND ELECTROPHYSIOLOGY OF THE NERVOUS SYSTEM

2.1. The structure of nerve cells

The fact that the nervous system is primarily concerned with sending and receiving messages to and from all parts of the body and processes enormous quantities of information imposes certain structural requirements upon the neurons. In the periphery, nerve cells have to reach all parts, yet they should not occupy a large proportion of the available space. In the central nervous system, enormous numbers of neurons have to coexist. Therefore, neurons have long, slender processes emanating from a cell body (Paul 1975).

2.2. The general shapes of neurons

Every neuron has a cell body (the soma or cyton) and sprouting from it are various cellular processes. The longest of these is usually the axon which runs almost the entire length of the neuron and connects, both physically and a functionally, the two terminal zones called the *dendron* and *telodendron*.

There are three types of neurons found in nervous systems Fig 2.1. The most common one is the multipolar Fig 2.1c and the least common one is the bipolar cell Fig 2.1.b, which is found primarily in the retina and cranial nerves supplying the cochlea, semicircular canals and vestibule. The third type Fig 2.1a is the monopolar cell which is found exclusively in ganglia just external to the spinal cord (Paul 1975).

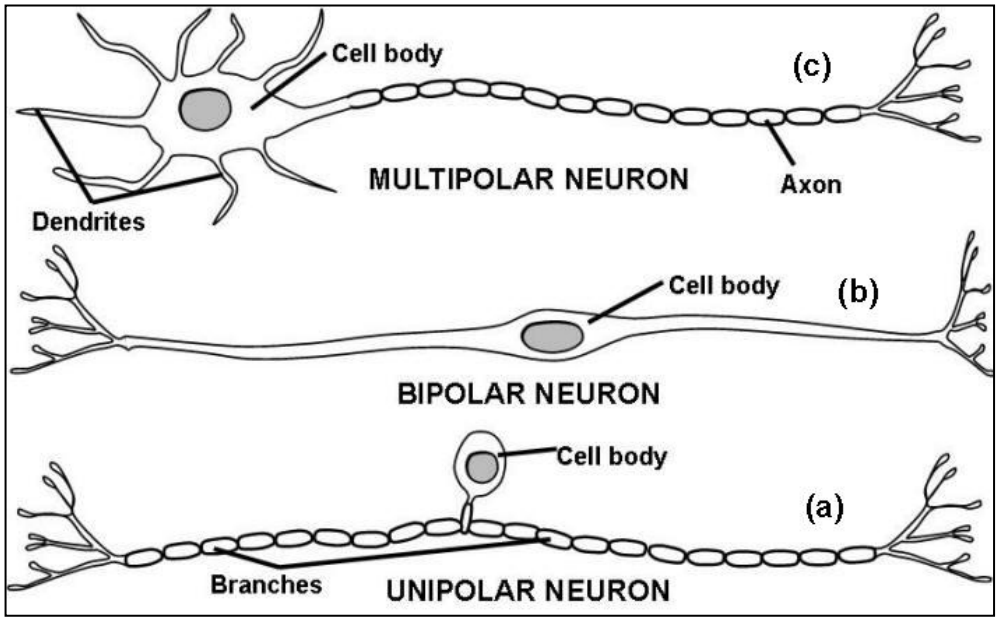

Figure 2.1. Diagram of the three main types of neuronal structure. (a) a unipolar neuron. (b) a bipolar neuron with the cell body straddling the axon; (c) a multipolar neurons in which the cell body from it (Paul 1975).

2.3. The axon

Axons are long, slender projection of neurons that conducts electrical impulses. During development, axons become associated with special nonnervous cells called *neuroglia*. These cells are known as *oligodendrocytes* in the central nervous system and *Schwann cells* in the periphery. Their main function is to support the axons and insulate them through *myelination* (Paul 1975).

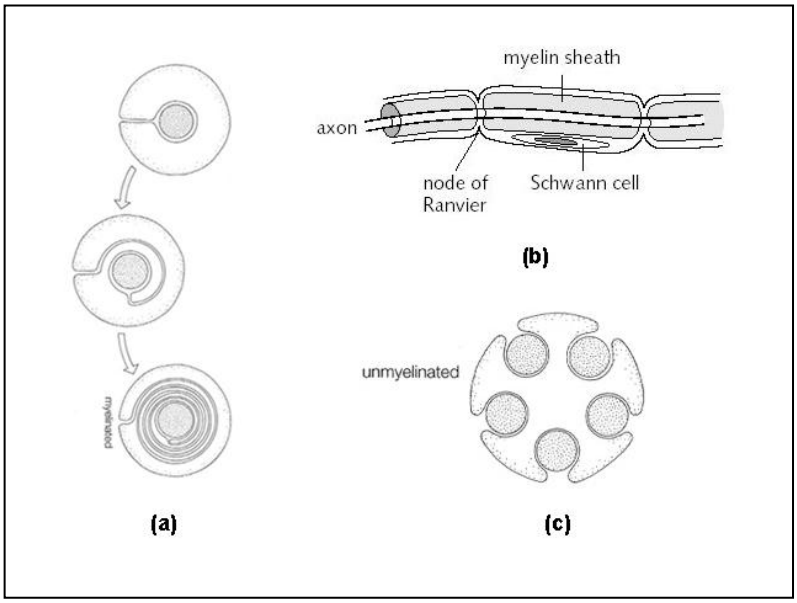

Figure 2.2. (a) development of the myelin sheath. The axon starts by lying in a groove in the Schwann cell. (b) the territory of one Schwann cell lies between two nodes of Ranivier. (c) Unmyelinated axons lying in grooves in an undifferentiated Schwann cell (Paul 1975).

Myelin is an insulating layer covering the axons of certain neurons. The main function of myelin is to increase the propagation speed of the nerve impulse. There are regular disruptions to the myelin sheath on the axon at spots called *node of Ranvier* Fig. 2.2. The axon (with or without a myelin sheath) is often referred to as a *nerve fiber*, a term that we use often in this work. In vertebrates the largest axons are myelinated and have a diameter of about 20 μm. Invertebrates do not have myelinated axons but the fibers may be very large indeed. Axon diameters of 100 μm are not uncommon and the giant axons from the mantle of the squid can be up to 800 μm in diameter. These huge axons have been extensively studied in experiments designed to reveal the basic mechanism involved in nerve excitability (Paul 1975).

2.4. The Dendron and the Telodendron

As it is a specialized region of a neuron to which other neurons are able to transmit messages, the dendron can be described as the receptive pole. It is usually a considerably branched structure, the individual branches being called *dendrites*. In

multipolar neurons, the main dendritic branches sprout directly from the soma (Paul 1975).

Just as the dendron is specialized to receive information, so the telodendron is specialized to transmit information. The telodendron is formed of the terminal branches of the axon, called telodendrites or, more commonly, axon terminals (Paul 1975).

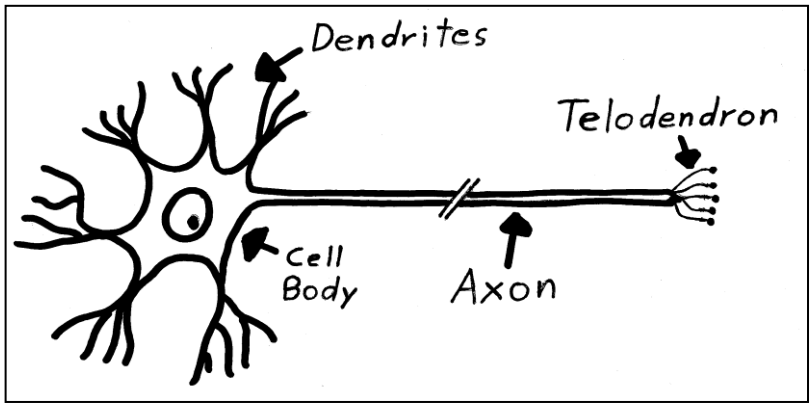

Figure 2.3. Shape of Dendron and telodentron in axon

2.5. Synapses

The region where an axon terminal contacts the cell membrane of another neuron is called a *synapse*. The vast majority of synapses occur between terminals and dendrites and to lesser extent cell bodies. There are, in some locations, synapses between axon terminals and axons, and even more rarely between dendrite and dendrite (Paul 1975).

In synapses where information transmission is achieved by chemical means, there is always a distinct gap, 10-20 nm wide, between the presynaptic and postsynaptic membranes which is termed the *synaptic cleft*.

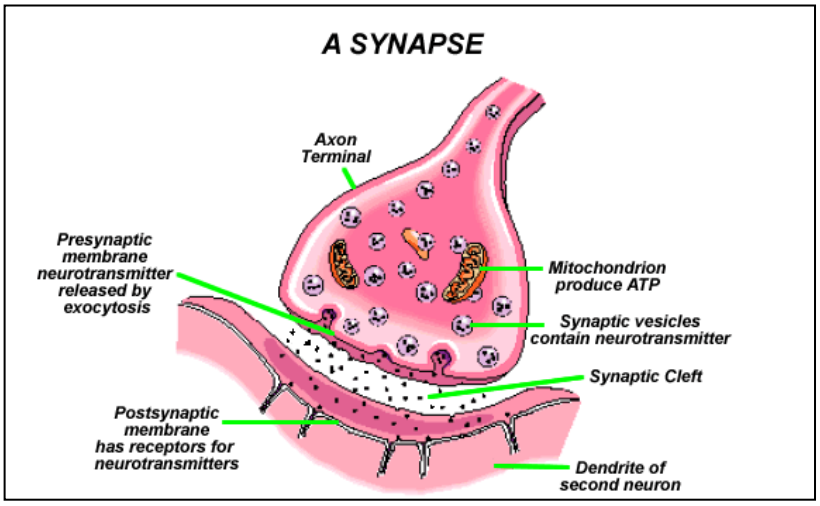

Figure 2.4. Structure of a synapse.

2.6. Membrane potential

In every living cell that has been investigated, a membrane potential has been demonstrated with the interior of the cell negatively charged with respect to the extracellular fluid. Because this potential difference across the membrane is maintained at a steady level when excitable cells are inactive, it is called the *resting potential*. This potential is maintained actively through proteins (called Na^+-K^+ *ATPase* or simply Na^+-K^+ *pump*) that are located on the cell membrane and pump intracellular Na^+ out and take extracellular K^+ in. Typically, a chemical or electrical effect may alter this equilibrium and an *action potential* is formed, which is explained in the next chapter.

Before the development of microelectrodes, the determination of the resting potential of a signal fiber could only be done in the large axons of the squid and it was from this giant fiber that Hodgkin and Huxley made the first classic measurements. They inserted an electrode into the axoplasm of one these fibers so that its tip was opposite and across the membrane from a second electrode on the outside of the wall. They found a potential difference in the resting nerve of approximately 50 mV (the inside of the membrane being negative to the outside). Very similar techniques were also being used by Cole and Curtis at this time with the same results. Since this pioneer work on recording from within the axon,

microelectrode techniques have been developed for penetrating and recording intracellular potentials from the cell bodies of neurons. This was first achieved in mammalian cell bodies of the large motor neurons of the spinal cord which are only some 70 μm in diameter. In their earlier work, Eccles and his colleagues used, as electrodes, glass capillaries filled with an electrolyte and with a tip diameter of 0.5 μm. Many types of even finer electrodes have since been developed by many workers throughout the world. In spinal motor neurons of the cat, Eccles found the difference in potential across the membrane to lie in a range of 60 to 80 mV. A similar order of transmembrane potential has been found for many cells (Paul 1975).

2.7. The Goldman Equation

Most biological components contain many types of ions including negatively charged proteins. The *Goldman equation* is used in cell membrane physiology to determine the equilibrium potential across a cell's membrane. For multiple ions, the ion flux through the membrane at the resting state is zero. For example, consider the three major ions involved in the nerve cell stimulation, Na^+, K^+, and Cl^- ions. Then,

$$V = -\frac{RT}{F} ln\left(\frac{P_k[K^+]_i + P_{Na}[Na^+]_i + P_{cl}[Cl^+]_o}{P_k[K^+]_o + P_{Na}[Na^+]_o + P_{cl}[Cl^+]_i}\right) \qquad (2.1.)$$

where R is the gas constant, F the Faraday constant and T the absolute temperature and P_{Na}, P_K, and P_{Cl} are the membrane permeability of Na^+, K^+, and Cl^- ions, respectively (Keener and Sneyd 2009).

2.8. The generation of an Action Potential

The resting potential of the neuronal membrane is about -70 mV. A stimulus, either electrical (like in an experiment) or chemical (like in vivo) excites the membrane and an action potential starts. Consider the ideal neuron illustrated in Fig 2.5. The membrane of a neuron has three types of transportation proteins: *sodium-*

potassium pumps, *potassium channels*, and *sodium channels*. The pumps work continuously to establish and maintain concentration gradients. Note that K^+ is concentrated twenty fold inside the cell and that Na^+ is concentrated tenfold outside the cell (Besr, Connors and Paradiso 2001).

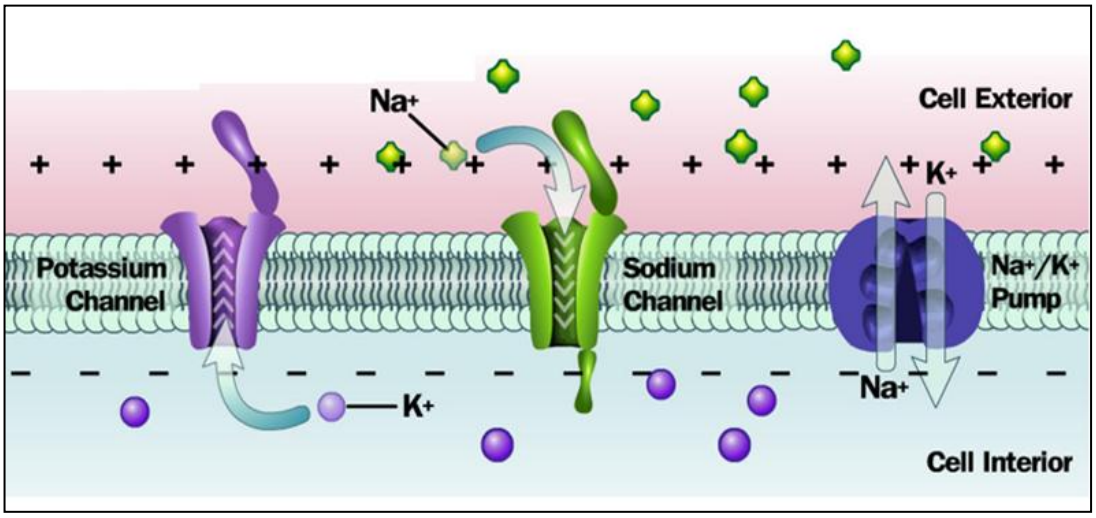

Figure 2.5. Here is an ideal neuron with sodium-potassium pumps, potassium channels, and sodium channels. The pumps establish ionic concentration gradients so that K^+ is concentrated inside the cell and Na^+ is concentrated outside the cell (Besr, Connors and Paradiso 2001).

The action potential occurs through the following steps:

STEP 1: *Depolarization to Threshold.* Before an action potential can begin, an area of excitable membrane must be depolarized. There is a threshold value for this depolarization that must be passed for an action potential to initiate. Otherwise, the action potential does not initiate.

STEP 2: *The Activation of Sodium Channels and Rapid Depolarization.* At threshold, the sodium activation gates open and the cell membrane becomes much more permeable to Na^+. Driven by the large electrochemical gradient, sodium ions rush into the cytoplasm, and rapid depolarization occurs at the site. In less than a millisecond, the inner membrane surface has changed; it now contains more positive ions than negative ones, and the transmembrane potential has changed from -60 mV to positive values closer to the equilibrium potential for sodium.

STEP 3: *The Inactivation of Sodium Channels and the Activation of Potassium Channels.* As the transmembrane potential approaches +30 mV the inactivation gates of the voltage regulated sodium channels begin closing. This step is known as *sodium channel inactivation*. While it is under way, voltage regulated potassium channels open. At a transmembrane potential of +30 mV the cytosol along the interior of the membrane contains an excess of positive charges. Thus, in contrast to the situation in the resting membrane, both the electrical and chemical gradients favor the movement of K^+ out of the cell. The sudden loss of positive charges then shifts the transmembrane potential back toward resting levels, and repolarization begins.

STEP 4: *The Return to Normal Permeability.* The voltage-regulated sodium channels remain inactivated until the membrane has repolarized to near threshold levels. At this time, they regain their normal status: closed, but capable of opening. The voltage-regulated potassium channels begin closing as the membrane reaches the normal resting potential (about -70 mV), but the process takes at least a millisecond. Over that period, potassium ions continue to move out of the cell at a faster rate than when they are at rest, producing a brief hyperpolarization that brings the transmembrane potential very close to the equilibrium potential for potassium (-90 mV). As the voltage-regulated potassium channels close, the transmembrane potential returns to normal resting levels. The membrane is now in a prestimulation condition, and the action potential is over (Besr, Connors and Paradiso 2001).

An action potential as it would appear on the display of an oscilloscope is shown in Fig 2.6. The event we have just described occurs in a single nerve fiber and thus called a *single fiber action potential* (SFAP).

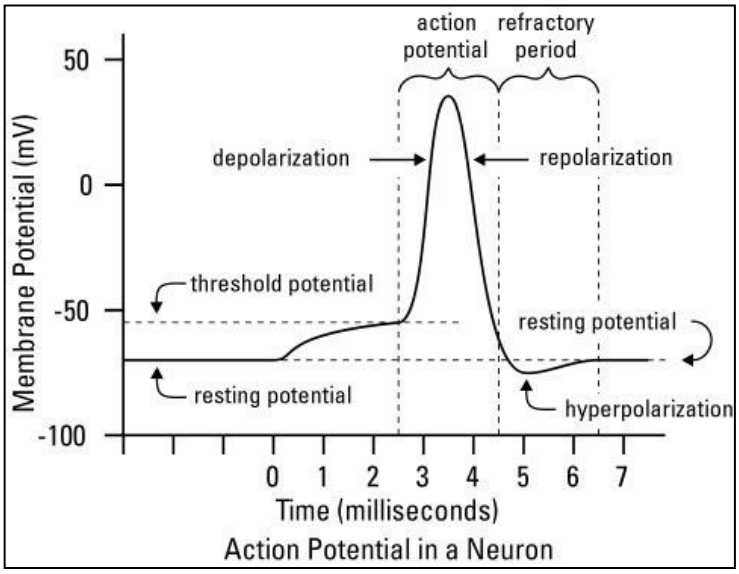

Figure 2.6. The parts of an action potential (Besr, Connors and Paradiso 2001).

3. MODELLING OF ACTION POTENTIAL

3.1. Activity of axon

It has long been known that activity in axons is accompanied by electrical changes in and around them. For this reason, the specific electrical event that occurs was called the *action potential*. Activity in axons takes the form of a series or train of discrete electrical events, each one being an individual action potential and the size of these potentials remains relatively constant as they are conducted along the axon (Paul 1975).

3.2. Conduction velocity

Conduction velocity is simply a matter of how far and how soon currents are sufficient to reach the fiber's threshold. Thus the factors that will influence this velocity are: how large the currents are, how high the threshold, how far they spread, and how long it takes them to depolarize the membranes. In the case of nerve fibers, the membrane is both a good insulator and extremely thin, and makes a splendid capacitor: it has a capacitance, of about 1 $\mu F/cm^2$ (Carpenter 1997).

In Fig 3.1 an equivalent circuit of the nerve membrane is shown, in order to explain the spread of the current from one part of the fiber to another.

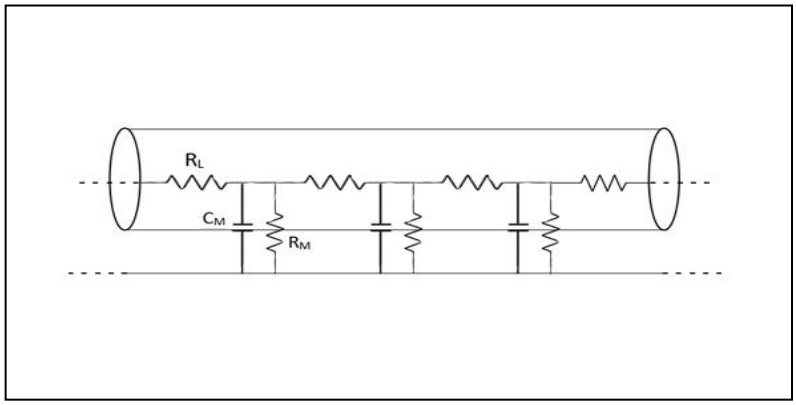

Figure 3.1. Equivalent circuit of the nerve membrane include membrane capacitance C_m as well as resistance R_m (Carpenter 1997).

Myelination thickens the layer of insulation around the fiber which has the desirable consquence of greatly increasing the resistance R_m and reducing the capacitance C_m. Since in myelinated fibers the sodium and potassium channels are virtually located at the Ranvier nodes, the action potential in effect jumps from node to node along the cytoplasm, giving rise to the term *saltatory conduction*. Cytoplasm offers resistance to ion movement, although much less resistance than the cell membrane. In this instance, an axon behaves like an electrical cable where a larger diameter leads to a lower resistance. In saltatory conduction, conduction velocity rises linearly with total fiber diameter (including the myelin) unlike to unmyelinated fibers where the velocity is proportional to the square root of the diameter. A consquence of this is that if we plot the velocity-diameter relationship for both types of fiber on the same graph Fig 3.2, the two curve cross over at a diameter near 1 μm. At this point the benefit of the myelin is exactly offset by the consequent reduction in axon diameter. So, there is no point in having myelinated fibers smaller than 1 μm in diameter or unmyelinated ones larger than this. This is eaxctly what is observed biologically in nerve fiber bundles (Carpenter 1997).

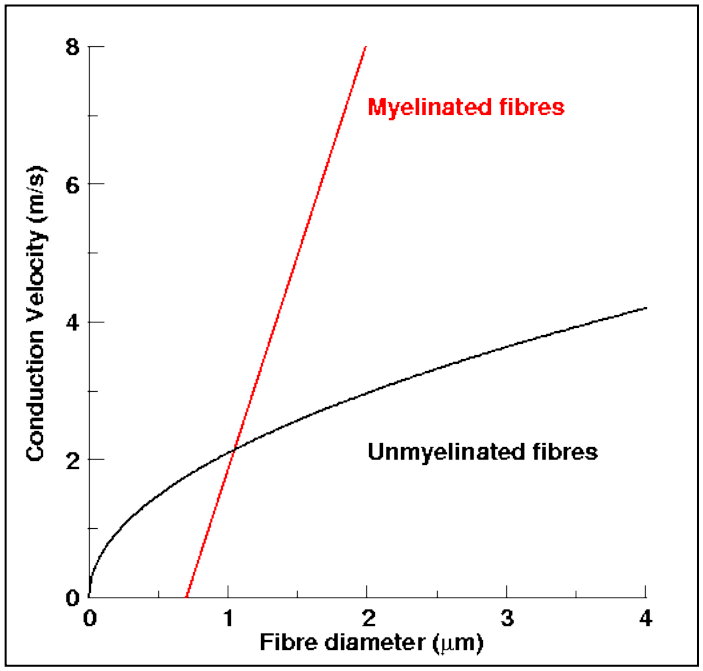

Figure 3.2. Theoretical dependence of conduction velocity on fiber diameter for unmyelinated and myelinated fibers (Carpenter 1997).

Axons are classified into three groups according to the relationships among the diameter, myelination, and propagation speed:

1. Type A fibers are the largest axons, with diameters ranging from 4 to 20 μm These are myelinated axons that carry action potentials at speeds of up to 140 meters per second.

2. Type B fibers are smaller myelinated axons, with diameters of 2-4 μm. Their propagation speeds average around 18 meters per second.

3. Type C fibers are unmyelinated and less than 2μm in diameter. These axons propagate action potentials at the leisurely pace of 1 meter per second.

There is even a subdivision within the A fibers. These have been according to size and conduction rate named α, β, γ, and δ fibers (Brazier 1977).

3.3. Compound action potentials

A single axon will generate an extracellular current. An easy way of increasing the signal available is to use large number of axons and make them become active simultaneously. A whole nerve contains many thousands of axons and

if an electrical pulse is applied of sufficient strength to excite all these axons simultaneously, their combined activity will generate a considerable extracellular current which can be easily recorded using a suitable set of electrodes. A recording obtained in this way is called a *compound action potential*.

On a descriptive level, we may say that when there is an adequate length of nerve between the stimulating and recording electrodes there are three major complexes following a shock to a nerve containing A, B and C type fibers. The A complex which comes first and which is by far the largest consists of a large negative potential followed by a smaller one and then later by a still smaller one as shown in Fig 3.3 (Brazier 1977).

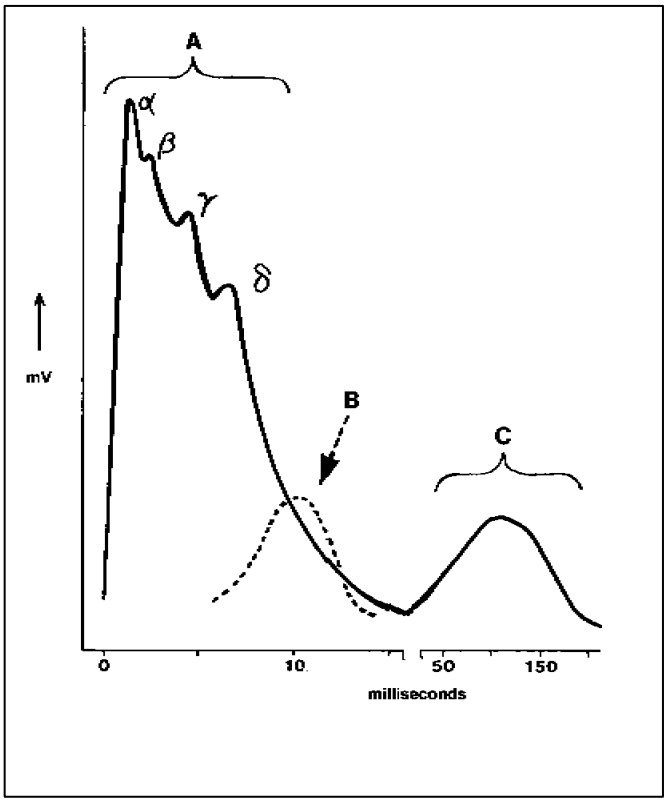

Figure 3.3. Reconstruction of a compound action potential. The A spike with its alpha and beta elevations is contributed by the fibers of the A group, the B elevation by the more slowly conducting fibers of the B group, and the C elevation by the slowest of all the fibers (Brazier 1977).

If the stimulus is not strong enough to excite all fibers, the resultant compound action potential will have a different curve owing to different levels of

excitability of the various fiber types; A fibers having a lower threshold of response than B fibers; and B lower than C. As can be seen in Fig 3.4, A mixed nerve having A and C fibers but no B fibers will give a compound action potential showing A and C elevations, but no B elevation (Brazier 1977).

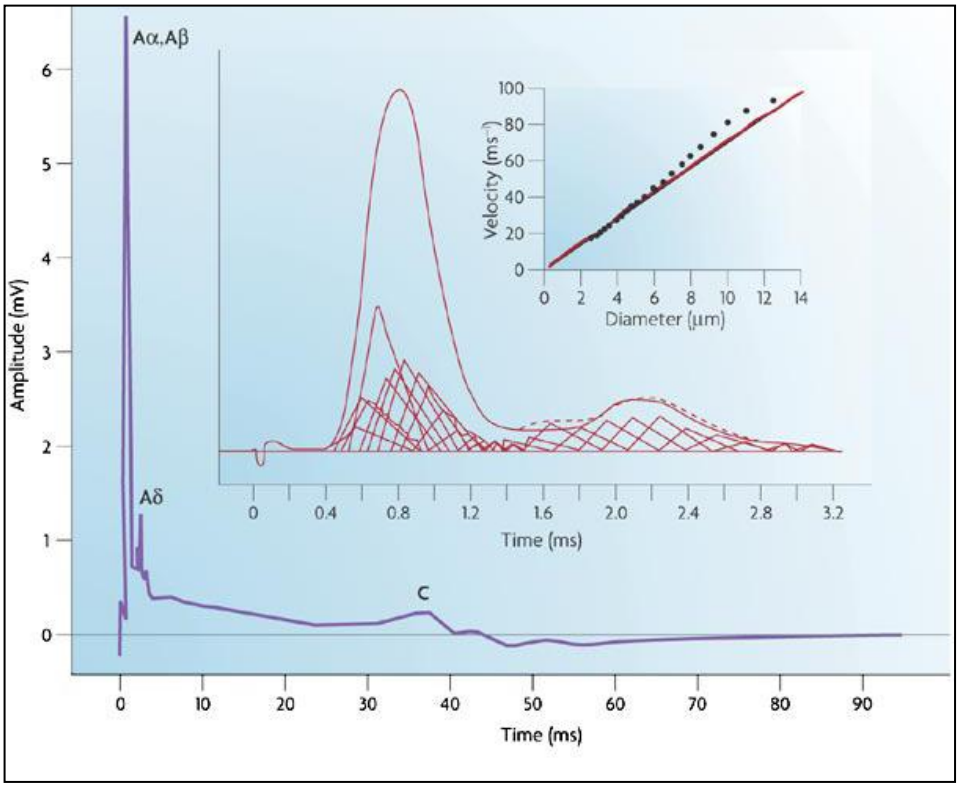

Figure 3.4. schematic representation of the compound action potential of a nerve with A and C fibers (Brazier 1977).

3.4. Simple experiments demonstrating compound action potentials

The arrangement that is employed to record a compound action potential is shown diagrammatically in Fig 3.5. The electrical stimulus is applied to the nerve through a pair of electrodes, labeled S_1 and S_2. The conducted action potential is recorded at a point relatively remote from the stimulating electrodes, using a second pair of electrodes (R_1 and R_2 in the diagram) (Paul 1975).

For simplicity, we can represent the electrical circuits by two resistances r_1 and r_2 and the system is arranged so that we measure the potential difference between the two electrodes R_1 and R_2 (Paul 1975).

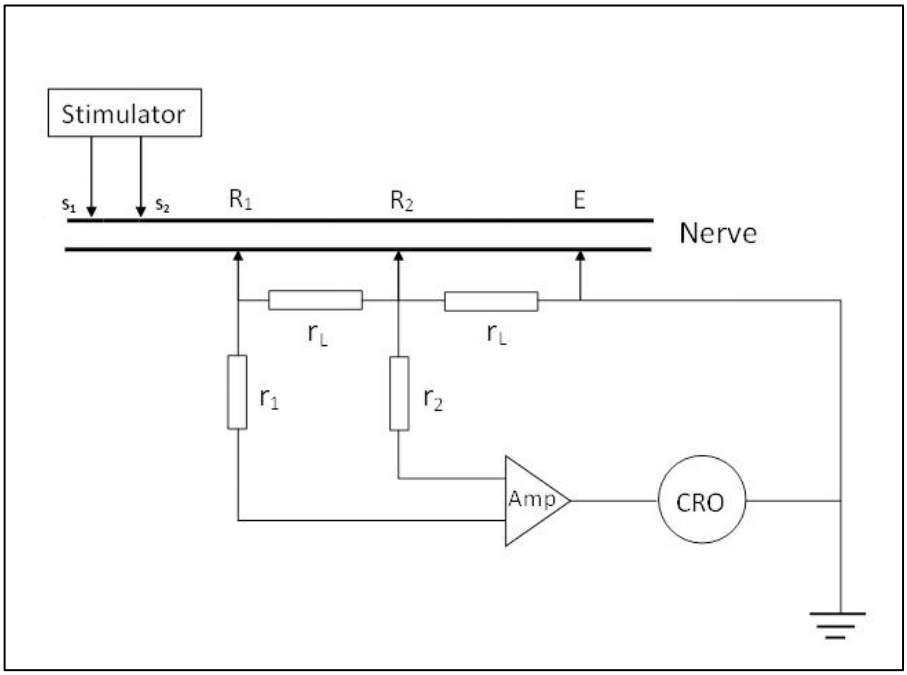

Figure 3.5. The experimental arrangement for recording a compound nerve action potential. Electrical pulses from the stimulator are applied to the nerve through the pair of electrodes S_1 and S_2. Activity is recorded from the nerve through the electrodes R_1 and R_2. The action potential signals are passed to an amplifier (amp) and displayed on a cathode ray oscilloscope (CRO). Between the stimulating and recording electrodes, a fifth electrode, E, is placed to conduct most of the stimulus current flowing in the extracellular fluid to earth. The resistances connecting R_1 and R_2 together (r_L) and the resistances r_1 and r_2 represent the input resistance of the amplifier. In order to record signals r_L must be high in relation to r_1 and r_2 (Paul 1975).

3.5. Measurement of conduction velocity from compound action potential

An approximate measure of the conduction velocity can be made by measuring the latent period and the length of nerve between the stimulating and recording electrodes, using the arrangement of Fig 3.5. Records are taken from two different points on the axon and the conduction velocity calculated from the distance between these two points and the difference between the latent periods of the two recordings. The experiment is illustrated in Fig 3.6. Recordings (a) and (b) are obtained from the points R_x and R_y on the nerve in (c). The distance between R_x and R_y is y-x. The time taken for the action potential to reach the recording electrodes

can now be estimated and in the diagram these times are marked as t_x and t_y. The conduction velocity can now be calculated as $y\text{-}x/t_y\text{-}t_x$ (Paul 1975).

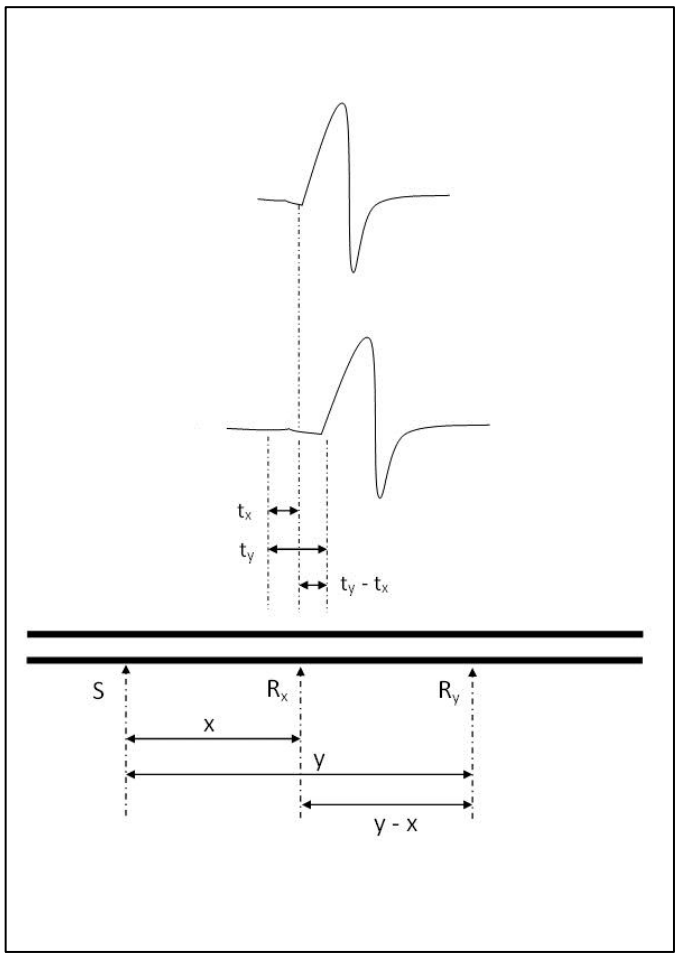

Figure 3.6. Measuring conduction velocity by difference method. (a) Record obtained at point R_x in (c); (b) Record obtained at point R_y in (c); (c) diagram of nerve end electrodes. Stimuli applied at S and recordings taken at R_x and R_y. Response latencies t_x and t_y are obtained from records (a) and (b). It is clear that the time taken for a response to travel the distance between R_x and R_y (y-x) is $t_x\text{-}t_y$. The conduction velocity is therefore $(y\text{-}x)/(t_x\text{-}t_y)$ (Paul 1975).

3.7. The Hodgkin–Huxley Model

The Hodgkin-Huxley Model describes the SFAP in an empirical way using the experimental data obtained by the same researchers. It is a complex model which describes the profile of SFAP precisely. For completeness, we give a brief summary of this model.

The circuit model of the cell membrane Fig 3.1.leads to the following differential equation (Keener and Sneyd 2009):

$$C_m \frac{dV}{dt} + I_{ion}(V,t) = 0 \qquad (3.6.)$$

where *V* denotes the cross-membrane potential. In the squid giant axon, as in many neural cells, the principal ionic currents are the Na^+ current and the K^+ current. Although there are other ionic currents, primarily the Cl^- current, in the Hodgkin–Huxley theory they are small and lumped together into one current called the *leakage current*. Since the instantaneous *I–V* curves of open Na^+ and K^+ channels in the squid giant axon are approximately linear, Eq.3.6 becomes

$$C_m \frac{dV}{dt} = -g_{Na}(V - V_{Na}) - g_k(V - V_k) - g_l(V - V_l) + I_{app} \qquad (3.7.)$$

where I_{app} is the applied current and g's are the conductance values of the individual ions. g's depend on three gating variables describing the behavior of voltage-dependent ion gates in the membrane. These gating variables are related with each other through a set of differential equations which further complicates the model. It is realistic to assume that the ionic concentrations, and hence the equilibrium potentials, are constant and unaffected by an action potential (Keener and Sneyd 2009). Eq. 3.7. is a first-order ordinary differential equation and can be written in the form:

$$C_m \frac{dV}{dt} = -g_{eff}(V - V_{eq}) + I_{app} \qquad (3.8.)$$

where $g_{eff} = g_{Na} + g_K + g_L$ and $V_{eq} = (g_{Na}V_{Na} + g_K V_K + g_L V_L)/g_{eff}$. V_{eq} is the membrane resting potential and is a balance between the reversal potentials for the three ionic currents. In fact, at rest, the Na^+ and leakage conductance are small compared to the K^+ conductance, so that the resting potential is close to the K^+ equilibrium potential (Keener and Sneyd 2009).

3.8. Modeling of compound action potential

When developing a model for the CAP, the first step is usually to propose a model for single fiber action potential (SFAP). Usually a triangular profile has been proposed for the SFAP considering its shape (Section 3.8.1.) (Gu, Gander and Chrichlow 1996). More recently, a smoother function has also been used to model SFAP (Dalkilic and Pehlivan 2002) which is also utilized in this work and described in the coming section. In both models, the profile of SFAP function has been modified according to fiber diameter.

The superposition of the SFAPs over the entire set of fibers to obtain the CAP is called a *forward problem*. If CAP is known and the fiber distribution resulting to this CAP is sought, then we have an *inverse problem* at hand.

3.8.1. The Forward Problem

The forward problem involves the determination of the CAP from a known CVD. It is known that CVD can be mathematically related to FDD. So, the forward problem can also be stated as the determination of CAP from a known FDD.

The solution of forward problem is usually straightforward. In order to derive the CAP from the fiber distribution, the following assumptions are made: (Dalkilic and Pehlivan 2002), (Schonhoven and Stegeman 1991)

1) The CAP can be represented as a linear superposition of its constituting elements, namely the SFAPs.

2) Action potentials propagate independently along different fibers. In other words, the action potential of one fiber does not affect the action potential in the neighboring fiber.

3) Upon electrical stimulation at a certain spot on the nerve, all fibers contributing to the CAP are activated simultaneously and instantaneously.

4) All fibers contributing to the CAP are activated at the same position along the nerve. The distance actually propagated by each individual spike is equal.

5) The propagation velocity of the action potential stays constant as it travels along the fiber.

Based on the above assumptions, CAP may be expressed in the discrete approach as:

$$CAP(t) = \sum_{i=1}^{M} w_i \, f_i(t - \tau_i) \qquad (3.9.)$$

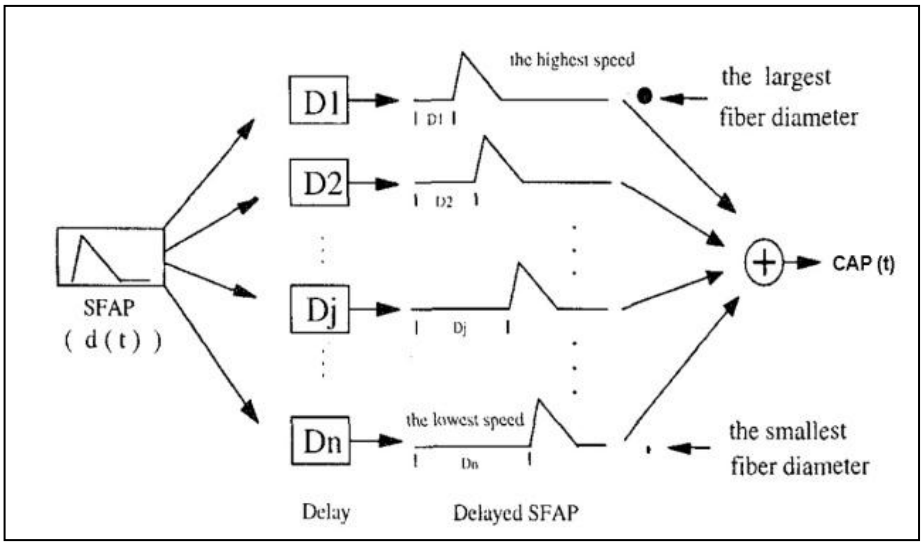

Figure 3.8. Generation of the compound action potential CAP (t) (adapted from Cummins et al. 1979, Dorfman, 1984 and Hirose et al. 1986). The smaller the fiber is in diameter, the slower is the SFAP.

Here *M* is the number of fiber groups categorized according to their diameter value. The SFAP waveform is described by the function $f_i(t)$ for group *i* whose shape

is also diameter dependent. The weighting coefficients (w_i) are parameters including the fiber population in the *ith* group and the diameter-dependent SFAP amplitude for this group of fibers. Thus, w_i may be expressed as

$$w_i = A_i . H_i \tag{3.10.}$$

where A_i is the amplitude of the SFAP and H_i is the number of fibers, both for the *i*th group (Cummins, Perkel et al. 1979). It is the delay of propagation for fibers in group *i* at the measurement site. τ_i is the time delay between the moment of stimulation and the passage of the SFAP of group *i* at the recording electrode (R. and Stegeman 1991) and expressed as

Note that the amplitude is expressed as a function of the fiber diameter as

$$\tau_i = \frac{l}{v_i} \tag{3.11.}$$

where v_i is the propagation velocity of fiber *i* and *l* is the distance between stimulation and recording electrodes.

$$A_i = \phi^p \tag{3.12.}$$

where ϕ the fiber diameter and *p* is a constant (Schonhoven and Stegeman 1991), (Waxman 1981).

The CAP model of Eq.3.9 can be formulated in discrete time by using equally spaced time samples for the SFAP and CAP function. Assuming that there are *K* values of the CAP for the k^{th} time point, the discrete values of observed *CAP* (t_k) depending on linear combination of single constituents from each conduction velocity class, is

$$CAP(t_k) = \sum_{i=1}^{M} H_i \ . \ f_i(t_k - \tau_i) \tag{3.13.}$$

Experiments show that the relationship between the external diameter of a myelinated fiber and conduction velocity is linear and can be expressed as

$$v = k\phi \tag{3.14.}$$

where ϕ denote the nerve fiber diameter. Using Eq.3.14, we can rewrite Eq. 3.11. as

$$\tau_i = \frac{l}{k\phi} \tag{3.15.}$$

To our knowledge, categorization of the fibers into a predefined number of groups is the only approach used in the related literature. Moreover, in most works histograms include only integer diameter values. On the other hand, it is obvious that a quantity like the diameter, which has a dimension of length, is of continuous nature. Considering the fact that a typical nerve contains a relatively high number of fibers (Schonhoven and Stegeman 1991), it is possible to express fiber population as a continuous distribution as a function of conduction velocity or the diameter value. In this case, the CAP can be expressed with an integral as:

$$CAP(t) = \int_{\emptyset_{min}}^{\emptyset_{max}} H(\phi)\, f\left(t - \frac{l}{k\phi}\right) d\phi \tag{3.16.}$$

Here, *H(Φ)* represents the FDD, i.e. the population density of fibers with a diameter value of *Φ*. It should be noted that

$$nf = \int_{\emptyset_{min}}^{\emptyset_{max}} H(\phi)\,.\,d\phi \tag{3.17.}$$

where *nf* indicates the total number of fibers.

3.8.2. The Inverse Problem

Inverse problem involves the estimation of CVD or FDD, represented by *H(Φ)* term in Eq. 3.16., from a given SFAP and CAP data.

In the inverse problem, one tries to achieve the inversion of the mathematical expression for the CAP. For the discrete case this inversion can be achieved in a couple of different ways (Schonhoven and Stegeman 1991).

For the continuous case, one possibility involves, again, the deconvolution of Eq.3.15 which deconvolution is used to reverse the effects of convolution on recorded data. This means that instead of mixing two signals like in convolution, we can isolate them. In this work, we have assumed certain functional forms for *H(Φ)* and determine the coefficients defining the function in a least squares sense, such that the square of the error between the simulated and measured results throughout the entire duration of the CAP measurement is minimized. In other words, the minimum of the time integral of the error square, namely,

$$E = \int_0^{t_{max}} (CAP(t) - CAPE(t))^2 \, . dt \qquad (3.18.)$$

has to be found. In Eq. 3.18, *CAPE (t)* represents the experimental CAP data. Using Eq. 3.16., Eq. 3.18. can be written as

$$E = \int_0^{t_{max}} \left[\left[\int_{\emptyset_{min}}^{\emptyset_{max}} H(\phi) f\left(t - \frac{l}{k\phi}\right) d\phi \right] - CAPE(t) \right]^2 dt \qquad (3.19.)$$

The minimization procedure will have different mathematical details depending on the function type chosen to represent *H(Φ)*, as described in the next chapter.

4. METHOD

4.1 Introduction

We will use a least squares approach to find the FDD, namely *H(Φ)*, with an assumed function type. Biologically, FDDs have specific shapes rather than arbitrary ones (Benno, et al. 1995). Two typical examples for FDD are given in Fig 4.1. and Fig 4.2.

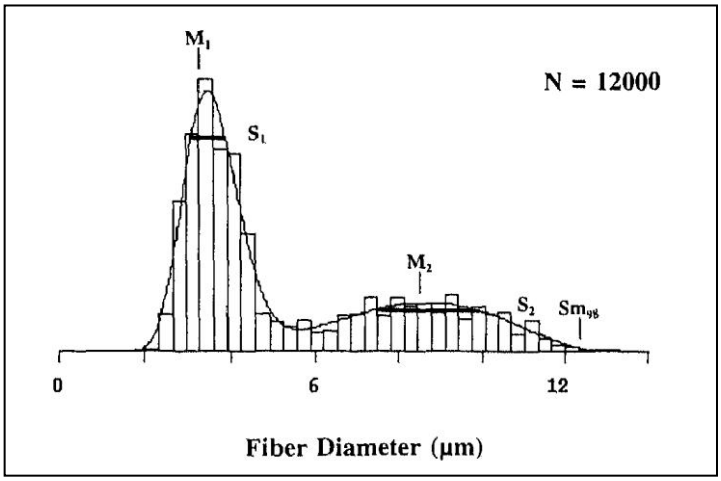

Figure 4.1. A typical example of a fiber diameter histogram for the sural nerve, obtained from morphological data (Benno, et al. 1995). The number of total fibers is 12000.

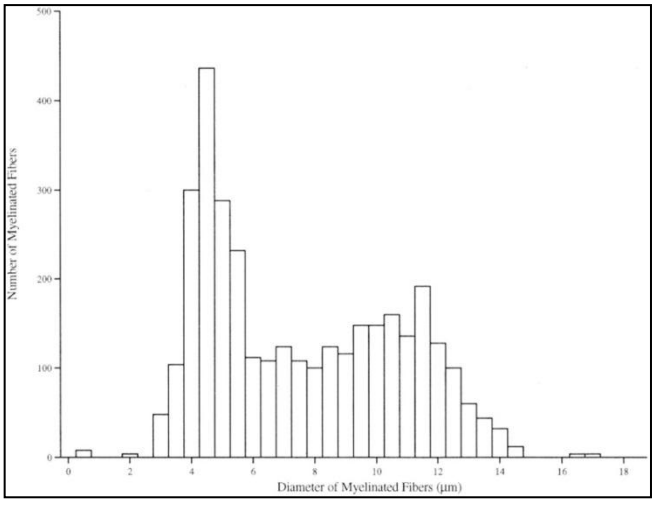

Figure 4.2. Diameter distribution myelinated fiber.

In particular, double Gaussian and polynomial curves seem to capture biological FDDs. In this chapter, we will describe the mathematical procedures for an assumed Gaussian and a polynomial distribution of fiber diameters leading to linear and nonlinear optimization problems, respectively.

First, we have assumed the single fiber action potential (SFAP) to be (Dalkilic and Pehlivan 2002)

$$f(t) = A.\sin\left(\frac{t}{\tau_1}\right) \cdot e^{\frac{-t}{\tau_2}} \qquad (4.1.)$$

where τ_1, and τ_2 are the parameters that mainly correspond to rising phase rate, and total duration of a SFAP, respectively. *A* represents an amplitude that scales the function. Note that τ_1, τ_2 and *A* depend on the fiber diameter value. The suggested function *f*(*t*) has two main advantages:

a) In most model studies, SFAP has been assumed as a triangle. A triangle has some sharp turnings, while our SFAP function has a continuous derivative function. This is not only closer to reality but also more convenient with respect to the optimization.

b) It has also a negative phase where the CAP falls below the baseline value at some point. This coincides with the negative phase observed in actual CAPs.

4.2. Optimization

We applied a least-squares optimization algorithm to find the minimum of Eq. 3.18. in order to estimate the fiber distribution *H (Φ)*. To achieve that, Eq. 3.18. has to be differentiated with respect to the coefficients of the assumed *H(Φ)* function. Suppose, the function *H (Φ)* has *n* unknown coefficients. In other words,

$$H\,(\Phi) = H\,(\Phi, \alpha_1, \alpha_2, \ldots, \alpha_n)$$

where α_i are the unknown coefficients to be determined. Least squares optimization leads to a set of *n* equations:

$$\frac{\partial E}{\partial \alpha_1} = 0 \quad , \quad \frac{\partial E}{\partial \alpha_2} = 0 \quad , \quad \ldots . \quad , \quad \frac{\partial E}{\partial \alpha_n} = 0 \qquad (4.2.)$$

Simultaneous solution of the above system will yield the optimal coefficients α_1-α_n and *H (*Φ*)* is found. Depending on the type of the assumed function, the system represented by Eq. 4.2 can be linear or nonlinear.

4.3. Gaussian distribution and nonlinear problem

One of the simplest possible approaches is to assume that the FDD is given as Gaussian distribution:

$$H(\mu, \sigma, \phi) = nf. \frac{1}{\sigma . \sqrt{2\pi}} . e^{\frac{-(\phi-\mu)^2}{2\sigma^2}} \qquad (4.3.)$$

In this case Eq.3.18. becomes:

$$E = \int_0^{t_{max}} \left[\left[\int_{\emptyset_{min}}^{\emptyset_{max}} H(\mu, \sigma, \phi) . f(t - t_d) d\phi \right] - CAPE(t) \right]^2 dt \qquad (4.4.)$$

To minimize the total square error, E, Eq.4.4 is differentiated with respect to μ and σ and the resulting expressions are set zero:

$$\frac{\partial E}{\partial \mu} = \int_0^{t_{max}} \left(\left[\int_{\phi}^{\phi_{max}} (f(t-t_d).H(\mu,\sigma,\phi) - CAPE).d\phi \right]. \left(\int_{\phi_{min}}^{\phi_{max}} f(t-t_d).\frac{\partial H}{\partial \mu}.d\phi \right) \right).dt = 0 \qquad (4.5.)$$

$$\frac{\partial E}{\partial \sigma} = \int_0^{t_{max}} \left(\left[\int_{\phi_{min}}^{\phi_{max}} (f(t-t_d).H(\mu,\sigma,\phi) - CAPE).d\phi \right]. \left(\int_{\emptyset_{min}}^{\emptyset_{max}} f(t-t_d).\frac{\partial H}{\partial \sigma}.d\phi \right) \right).dt = 0 \qquad (4.6.)$$

where $\frac{\partial H}{\partial \mu}$ and $\frac{\partial H}{\partial \sigma}$ are:

$$\frac{\partial H}{\partial \mu} = \frac{\phi - \mu}{\sigma^3.\sqrt{2\pi}} . e^{\frac{-(\phi-\mu)^2}{2\sigma^2}} \qquad (4.7.)$$

$$\frac{\partial H}{\partial \sigma} = \frac{(\phi-\mu)^2}{\sigma^4.\sqrt{2\pi}} . e^{\frac{-(\phi-\mu)^2}{2\sigma^2}} - \frac{1}{\sigma^2.\sqrt{2\pi}} . e^{\frac{-(\phi-\mu)^2}{2\sigma^2}} \qquad (4.8.)$$

It is also possible to use a double Gaussian curve to represent the FDD.

$$nf(\mu,\sigma,\phi) = \frac{nf}{2} . \left(\frac{1}{\sigma_1 . \sqrt{2\pi}} . e^{\frac{-(\phi-\mu_1)^2}{2{\sigma_1}^2}} + \frac{1}{\sigma_2 . \sqrt{2\pi}} . e^{\frac{-(\phi-\mu_2)^2}{2{\sigma_2}^2}} \right) \qquad (4.9.)$$

In this case, we have initially assumed *H(Φ)* to have four unknown coefficients, namely μ_1, μ_2, σ_1 and σ_2. However, this assumption results to convergence problems in the solution step. Instead, μ_1 and μ_2 are assumed to be known and optimization is performed with respect to σ_1 and σ_2.

The nonlinear system is obtained then in a similar way.

To solve the nonlinear systems we have used the well-known Newton-Raphson scheme which is briefly described here.

4.3.1. Newton-Raphson method

The simplest means of finding the root of a nonlinear equation system, is the Newton–Raphson method. It works well with simultaneous equations, provided that it is supplied with a good initial guess. There are other methods that have better global convergence characteristics, but all of them are variants of the Newton–Raphson method (Kiusalaas 2005).

Let $\boldsymbol{f(x)=0}$ represent the nonlinear equation system with $\boldsymbol{f}$ and $\boldsymbol{x}$ indicating the vector of equations and unknowns, respectively. In order to derive the Newton–Raphson method for a system of equations, we start with the Taylor series expansion of $\boldsymbol{f}$ about the vector $\boldsymbol{x}$:

$$\boldsymbol{f}(\boldsymbol{x}+\Delta\boldsymbol{x}) = \boldsymbol{f}(\boldsymbol{x}) + \sum_{j=1}^{N} \frac{\partial \boldsymbol{f}}{\partial \boldsymbol{x}} \Delta\boldsymbol{x} + O(\Delta\boldsymbol{x}^2) \qquad (4.10.)$$

Dropping terms of order $\Delta\boldsymbol{x}^2$, we can write Eq. (4.10.) as

$$\boldsymbol{f}(\boldsymbol{x}+\Delta\boldsymbol{x}) = \boldsymbol{f}(\boldsymbol{x}) + \boldsymbol{J}(\boldsymbol{x})\Delta\boldsymbol{x} \qquad (4.11.)$$

where $\boldsymbol{J(x)}$ is the Jacobian matrix (of size n× n) made up of the partial derivatives

$$J_{ij} = \frac{\partial f_i}{\partial x_j} \qquad (4.12.)$$

Note that Eq.4.11 is a linear approximation (vector $\Delta\boldsymbol{x}$ being the variable) of the vector-valued function $\boldsymbol{f}$ in the vicinity of point $\boldsymbol{x}$.

Let us now assume that $\boldsymbol{x}$ is the current approximation of the solution of $\boldsymbol{f(x) = 0}$, and let $\boldsymbol{x_{i+1}=x_i + \Delta x_i}$ be the improved solution. To find the correction $\Delta \boldsymbol{x}$, we set $\boldsymbol{f(x + \Delta x) = 0}$.

In Eq. 4.12 the result is a set of linear equations for $\Delta \boldsymbol{x}$:

$$\boldsymbol{J(x)\Delta x = -f(x)} \qquad (4.13.)$$

The following steps constitute the Newton–Raphson method for simultaneous, nonlinear equations: (Kiusalaas 2005)

1. Estimate the solution vector $\boldsymbol{x}$.
2. Evaluate $\boldsymbol{f(x)}$.
3. Compute the Jacobian matrix $\boldsymbol{J(x)}$ from Eq. 4.12.
4. Set up the simultaneous equations in Eq. 4.12 and solve for $\Delta \mathbf{x}$.
5. Let $\boldsymbol{x \leftarrow x + \Delta x}$ and repeat steps 2–5.

The above process is continued until $|\Delta \boldsymbol{x}| < \varepsilon$, where ε is the error tolerance. As in the one-dimensional case, success of the Newton–Raphson procedure depends entirely on the initial estimate of $\boldsymbol{x}$. If a good starting point is used, convergence to the solution is very rapid. Otherwise, the results are unpredictable (Kiusalaas 2005).

In the Gaussian distribution problem we have two equations to solve simultaneously:

$$r_1 = \frac{\partial E}{\partial \mu} = 0 \qquad and \qquad r_2 = \frac{\partial E}{\partial \sigma} = 0 \qquad (4.14.)$$

which results to the iterative scheme

$$\begin{bmatrix} \mu_{i+1} \\ \sigma_{i+1} \end{bmatrix} = \begin{bmatrix} \mu_i \\ \sigma_i \end{bmatrix} - \begin{bmatrix} \frac{\partial r_1}{\partial \mu} & \frac{\partial r_1}{\partial \sigma} \\ \frac{\partial r_2}{\partial \mu} & \frac{\partial r_2}{\partial \sigma} \end{bmatrix}^{-1} \cdot \begin{bmatrix} r_1(\mu_i\,,\,\sigma_i) \\ r_2(\mu_i\,,\,\sigma_i) \end{bmatrix} \qquad (4.15.)$$

4.4. Polynomial distribution and linear problem

It is also possible to assume a polynomial distribution for *H(Φ)* where the coefficients of polynomial terms are the unknowns to be found through optimization. In this problem, the resulting system is linear and can be solved directly without an iterative method.

We have tried polynomials of different orders, namely 3rd, 4th, 6th and 8th order, to represent FDD. The basic principle of the method is independent of the polynomial order chosen. Here, we illustrate the approach using a 6th order polynomial.

Suppose that FDD is given as

$$H(\phi) = a\phi^6 + b\phi^5 + c\phi^4 + d\phi^3 + e\phi^2 + f\phi + g \qquad (4.16.)$$

where *a*, *b*, *c*, *d*, *e*, *f* and *g* are the parameters to be determined.

We need to apply three constraints to this function.

1) $H(\phi_{min}) = 0$. This condition sets the minimum diameter, ϕ_{min}, present in the distribution.

2) $H(\phi_{max}) = 0$. This condition sets the maximum diameter ϕ_{min}, present in the distribution.

3) $\int_{\phi_{min}}^{\phi_{max}} H(\phi).d\phi = total\ number\ of\ fibers = nf$ This condition makes sure that the area under the *H(Φ)* curve equals to the total number of fibers present in the nerve.[1]

1. This condition does not have to be enforced in nonlinear problem since the area under the Gaussian distribution is always 1 (100 percent). Consequently, we can directly multiply *nf* with this curve.

These three constraints are imposed to $H(\Phi)$ before the optimization scheme. As a result, only 4 out of 7 unknown parameters are unconstrained and to be found through optimization.

For example, assuming $\Phi_{min}=0$ mm and $\Phi_{max}=20$ mm, the first two constraints give:

1) $H(0)=0 \rightarrow g=0$

2) $H(20)=0 \rightarrow f= - (a20^5+b20^4+c20^3+d20^2+e20)$

Substituting the expressions for g and f into Eq. 4.16. gives:

$$H(\phi) = (\phi^6 - 20^5\phi)a + (\phi^5 - 20^4\phi)b + (\phi^4 - 20^3\phi)c + (\phi^3 - 20^2\phi)d + (\phi^2 - 20\phi)e$$

Third constraints is directly applied to the above form:

3) $\int_0^{20} H(\phi).d\phi = nf \quad \rightarrow \quad m_1 a + m_2\, b + m_3\, c + m_4\, d + m_5\, e = nf$

So,

$$e = \frac{nf - m_1 a - m_2 b - m_3 c - m_4 d}{m_5}$$

where,

$$m_1 = \int_0^{20} (\phi^6 - 20^5\phi)d\phi \qquad (4.17.)$$

$$m_2 = \int_0^{20} (\phi^5 - 20^4\phi)d\phi \qquad (4.18.)$$

$$m_3 = \int_0^{20} (\phi^4 - 20^3\phi)d\phi \tag{4.19.}$$

$$m_4 = \int_0^{20} (\phi^3 - 20^2\phi)d\phi \tag{4.20.}$$

$$m_5 = \int_0^{20} (\phi^2 - 20\phi)d\phi \tag{4.21.}$$

After imposing the third constraint, *H(Φ)* becomes:

$$\begin{aligned} H(\phi) = &\left(\phi^6 - 20^5\phi - (\phi^2 - 20\phi)(\frac{m_1}{m_5})\right)a + \left(\phi^5 - 20^4\phi - (\phi^2 - 20\phi)(\frac{m_2}{m_5})\right)b \\ &+ \left(\phi^4 - 20^3\phi - (\phi^2 - 20\phi)(\frac{m_3}{m_5})\right)c \\ &+ \left(\phi^3 - 20^2\phi - (\phi^2 - 20\phi)(\frac{m_4}{m_5})\right)d \\ &+ \left((\phi^2 - 20\phi)\left(\frac{nf}{m_5}\right)\right) \end{aligned} \tag{4.22.}$$

The optimization is performed on Eq.4.22. by finding the optimal values for *a*, *b*, *c* and *d*.

Now we substitute Eq. (4.22) to Eq. (4.4) for finding these 4 unknown variables. Similar to what is done in the nonlinear problem, to minimize the total square error. Eq.4.4 is differentiated with respect to *a*, *b*, *c* and *d* and the resulting expressions are set zero:

$$\frac{\partial E}{\partial a} = \int_0^{t_{max}} \left(\left[\int_{\phi_{min}}^{\phi_{max}} (f(t-t_d).H(\phi) - CAPE).d\phi \right]. \left(\int_{\phi_{min}}^{\phi_{max}} f(t-t_d).\frac{\partial H}{\partial a}.d\phi \right) \right).dt = 0 \qquad (4.23.)$$

$$\frac{\partial E}{\partial b} = \int_0^{t_{max}} \left(\left[\int_{\phi_{min}}^{\phi_{max}} (f(t-t_d).H(\emptyset) - CAPE).d\emptyset \right]. \left(\int_{\phi_{min}}^{\phi_{max}} f(t-t_d).\frac{\partial H}{\partial b}.d\phi \right) \right).dt = 0 \qquad (4.24.)$$

$$\frac{\partial E}{\partial c} = \int_0^{t_{max}} \left(\left[\int_{\phi_{min}}^{\phi_{max}} (f(t-t_d).H(\phi) - CAPE).d\phi \right]. \left(\int_{\phi_{min}}^{\phi_{max}} f(t-t_d).\frac{\partial H}{\partial c}.d\phi \right) \right).dt = 0 \qquad (4.25.)$$

$$\frac{\partial E}{\partial d} = \int_0^{t_{max}} \left(\left[\int_{\phi_{min}}^{\phi_{max}} (f(t-t_d).H(\phi) - CAPE).d\phi \right]. \left(\int_{\phi_{min}}^{\phi_{max}} f(t-t_d).\frac{\partial H}{\partial d}.d\phi \right) \right).dt = 0 \qquad (4.26.)$$

Where derivatives of *H* with respect to *a*, *b*, *c* and *d* are equal to:

$$\frac{\partial H}{\partial a} = \phi^6 - 20^5\phi - (\phi^2 - 20\phi)\left(\frac{m_1}{m_5}\right) \qquad (4.27.)$$

$$\frac{\partial H}{\partial b} = \phi^5 - 20^4\phi - (\phi^2 - 20\phi)\left(\frac{m_2}{m_5}\right) \qquad (4.28.)$$

$$\frac{\partial H}{\partial c} = \phi^4 - 20^3\phi - (\phi^2 - 20\phi)\left(\frac{m_3}{m_5}\right) \tag{4.29.}$$

$$\frac{\partial H}{\partial d} = \phi^3 - 20^2\phi - (\phi^2 - 20\phi)\left(\frac{m_4}{m_5}\right) \tag{4.30.}$$

Now we have a linear system of equations in four unknowns, which can be solved easily. It should be noted that all integrals given in this section are evaluated numerically in the MATLAB implementation.

5. RESULTS

5.1. Introduction

To our knowledge, there is no study in the literature where CAP and FDD data for a specific nerve exists simultaneously. Hence, we have performed *numerical experimentation* where the "experimental" CAP data is produced by running the forward problem simulation with a specific FDD. The produced CAP data is then fed into the inverse problem simulation as if it originates from an actual experiment. The calculated FDD is then compared with the FDD assumed in the forward problem to check the effectiveness of the method. This methodology is commonly practiced in inverse problems that are encountered in different fields of science and engineering.

5.1. Results of nonlinear problem

A hypothetical, single peak FDD is assumed and the resulting CAP is (Fig. 5.1) is calculated in the forward problem. By processing the resulting CAP data, the inverse problem is able to fit an appropriate Gaussian curve to the assumed FDD (Fig. 5.2). It should be noted that the assumed FDD is not an exact Gaussian curve which only bears a visual similarity to it.

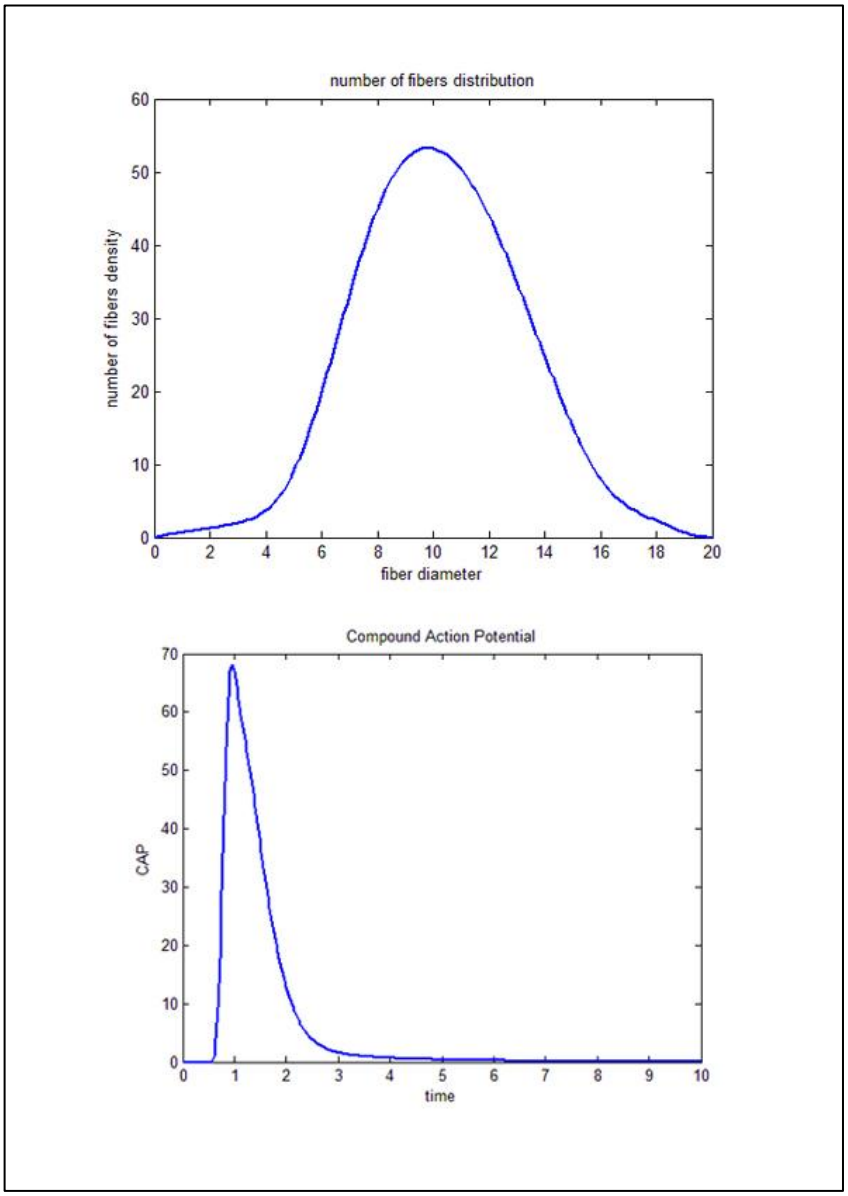

Figure 5.1. Experimental fiber diameter distribution and compound action potential, respectively.

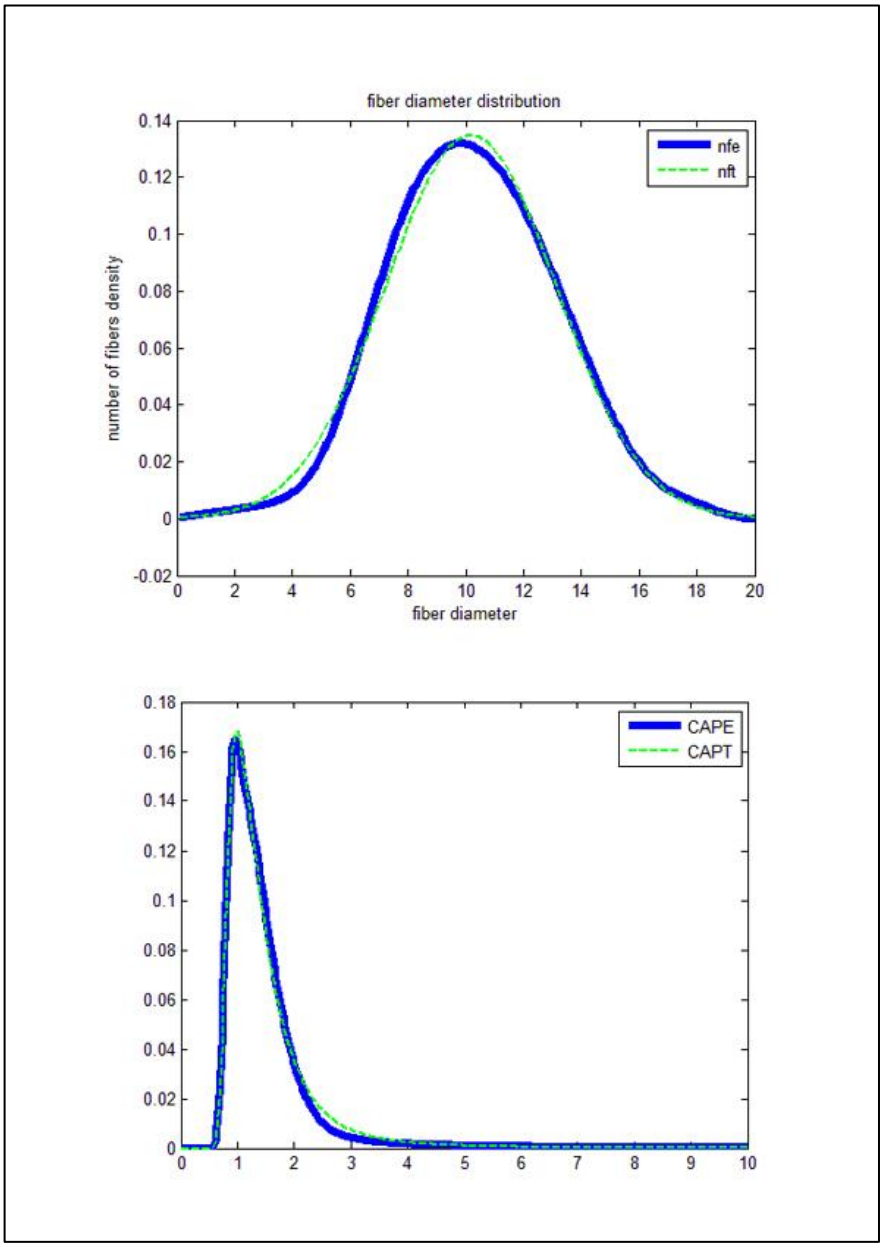

Figure 5.2. Calculated fiber diameter distribution and compound action potential with Gaussian function at distance 2 cm.

With known μ values and exact double Gaussian curve, the computed FDD matched well with that produced in the inverse problem (Fig. 5.3). However, we have experienced convergence problems if the curve deviates significantly from the form given in Eq.4.9.

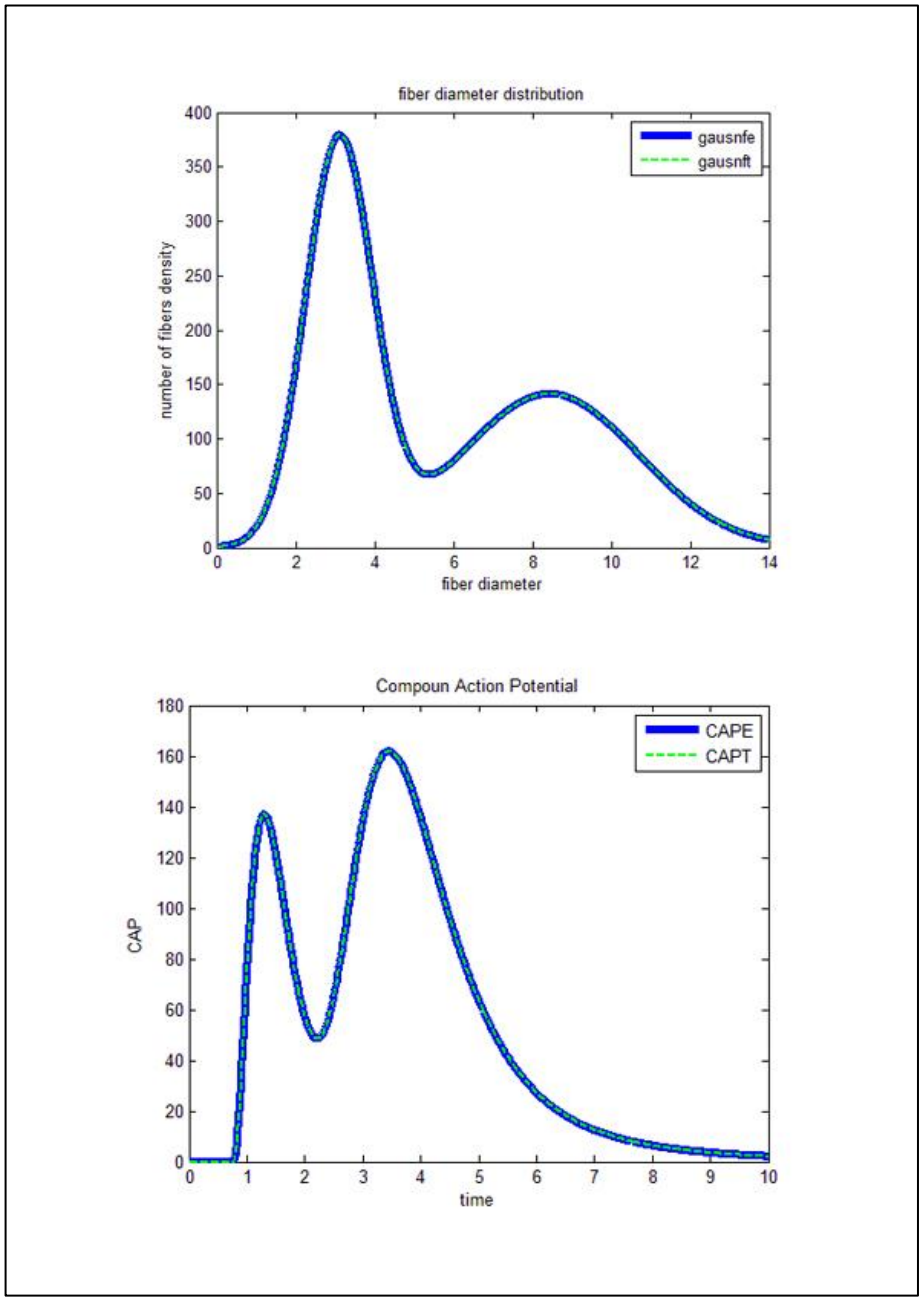

Figure 5.3. Calculated fiber diameter distribution and compound action potential with double Gaussian functions distribution nonlinear problem at distance 2 cm.

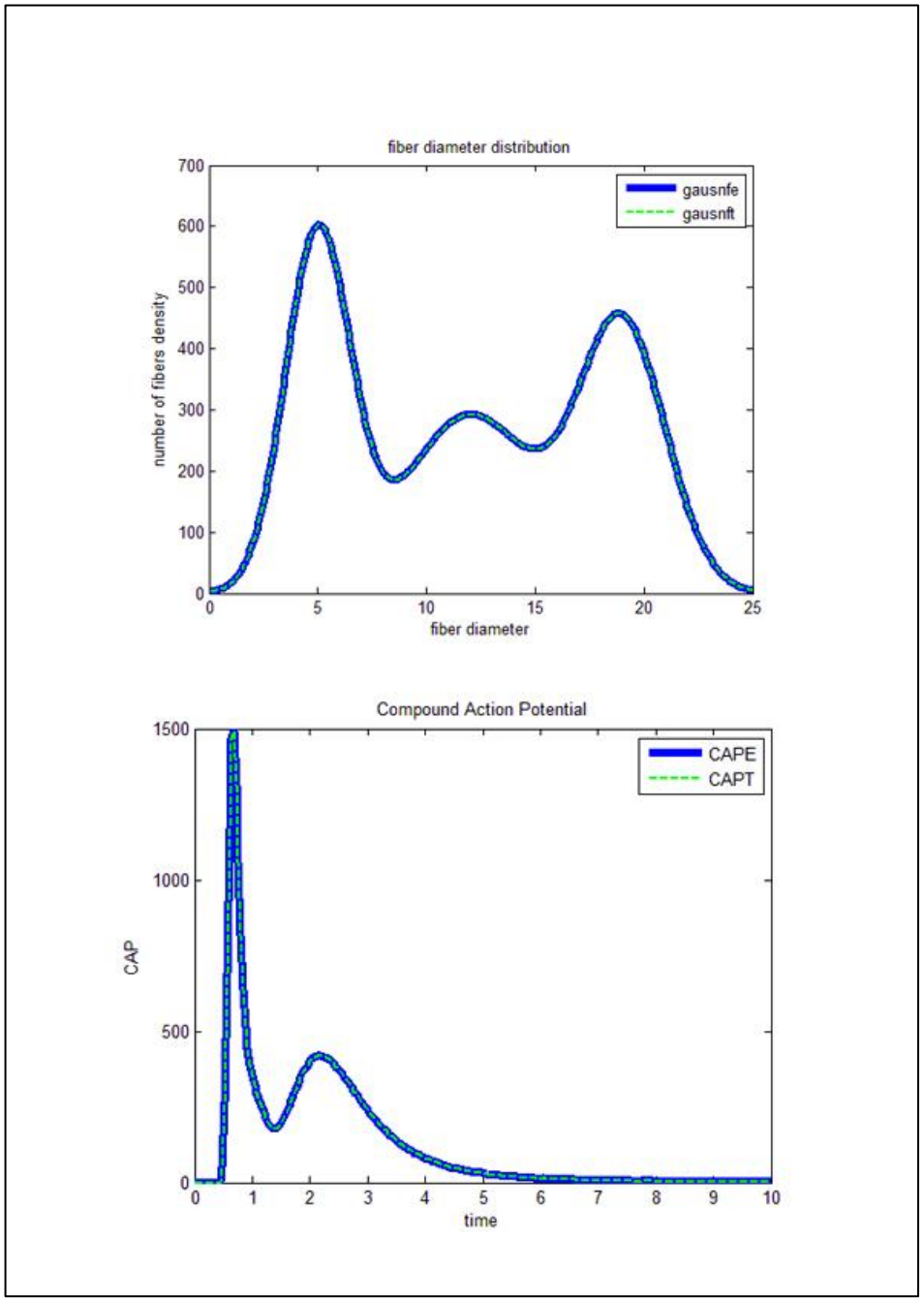

Figure 5.4. Calculated FDD and CAP with combination of three Gaussian functions distribution at distance 2 cm.

5.2. Result of linear problem

In the polynomial approach, 6^{th} and 8^{th} order polynomials have given good results and the following examples include only these.

In the hypothetical single peak distribution, the produced CAP data based on the assumed FDD (Fig 5.5) has been nicely captured by the 6^{th} (Fig. 5.6) and 8^{th} (Fig. 5.7) polynomials. As expected, 8^{th} order polynomial has slightly outperformed the 6^{th} order one in this example.

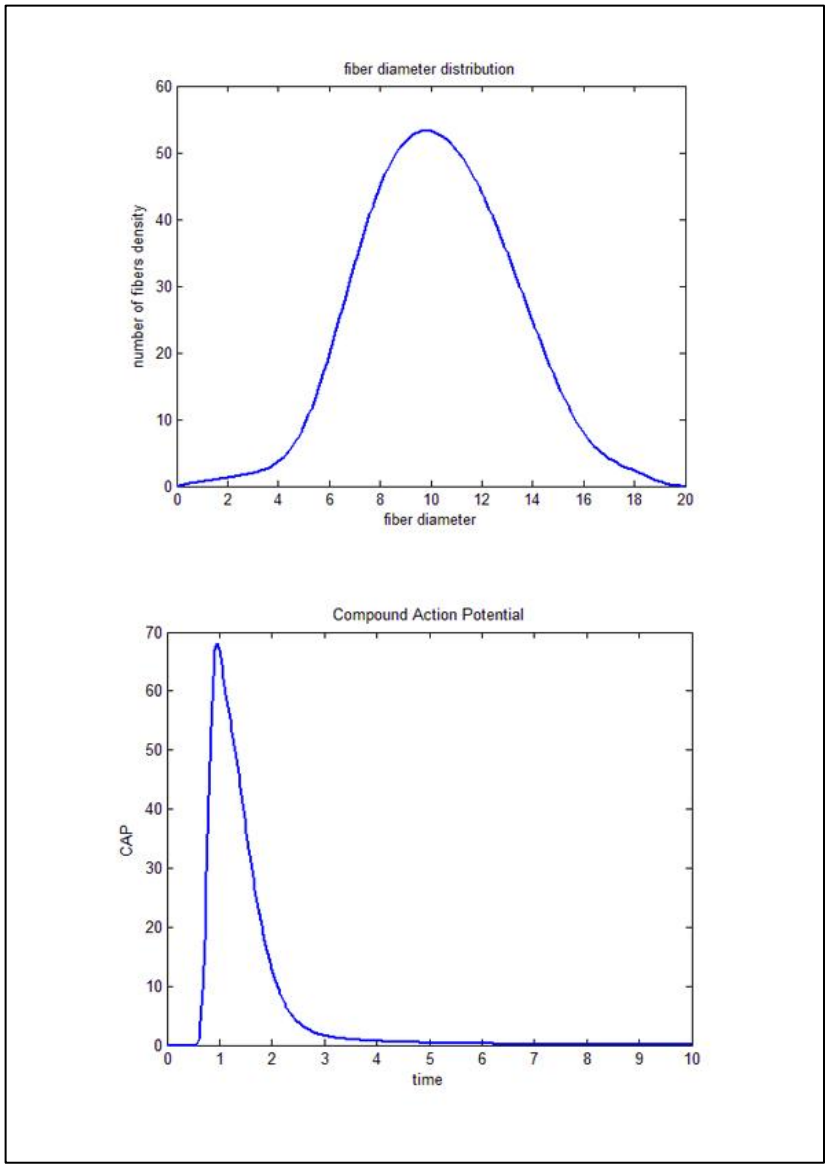

Figure 5.5. Experimental fiber diameter distribution and compound action potential, respectively.

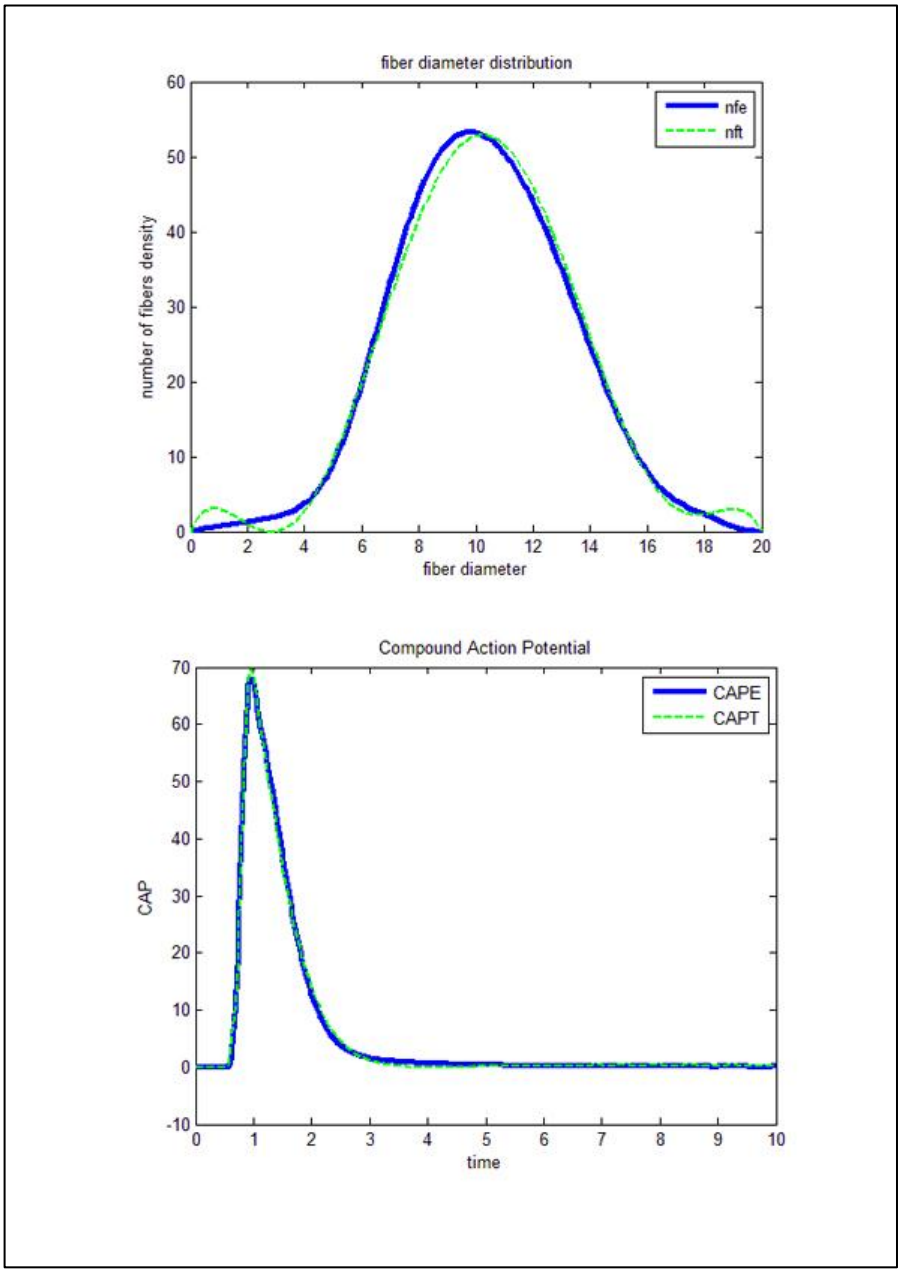

Figure 5.6. Calculated fiber diameter distribution and compound action potential with 6^{th} order polynomial at distance 2 cm.

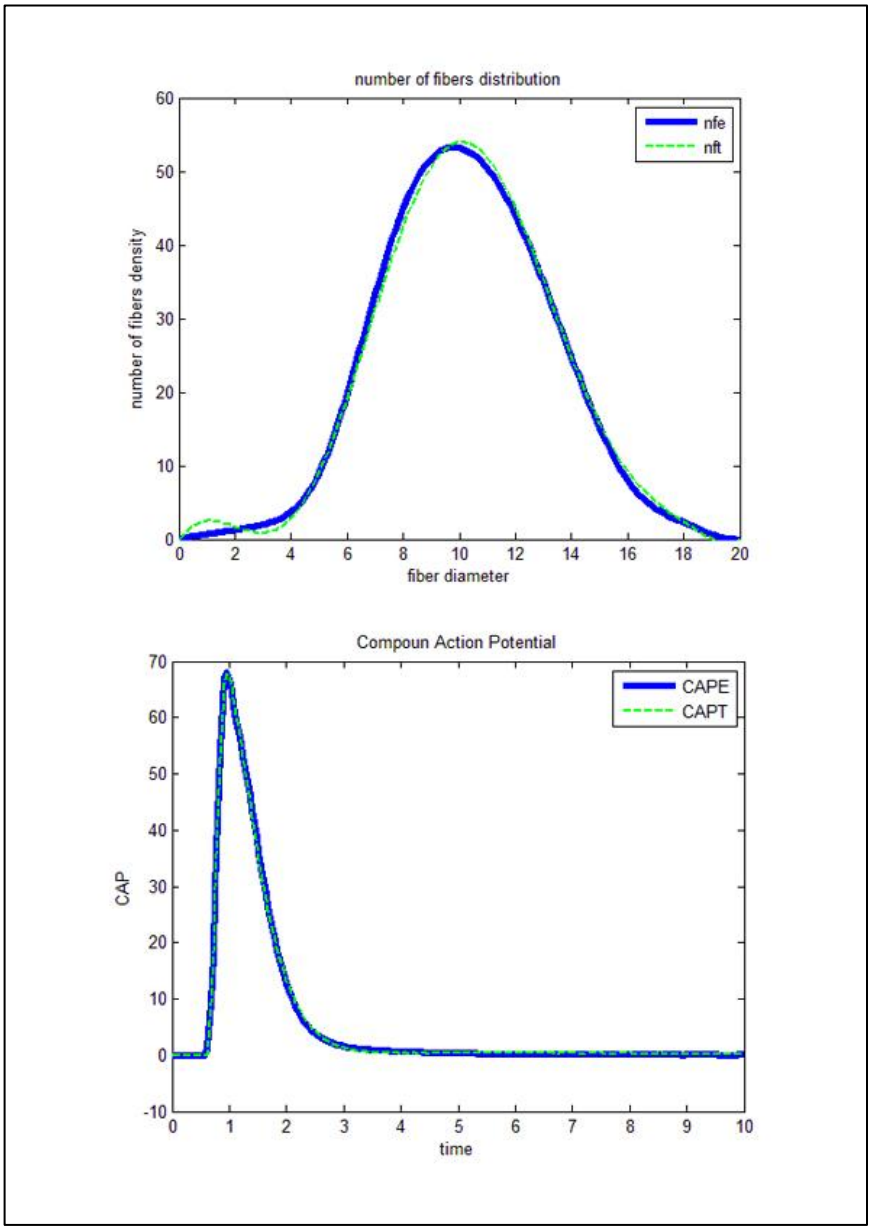

Figure 5.7. Calculated fiber diameter distribution and compound action potential with 8th order polynomial at distance 2 cm.

In the next example, we have taken an actual FDD belonging to the sural nerve of human, which has a typical double peak form.

In this example, the produced CAP (Fig. 5.8) has been well captured by the 6th order polynomial, although we have seen some error in the predicted FDD compared to the assumed one (Fig. 5.9). The 8th order polynomial have predicted both the CAP and FDD data accurately (Fig 5.10).

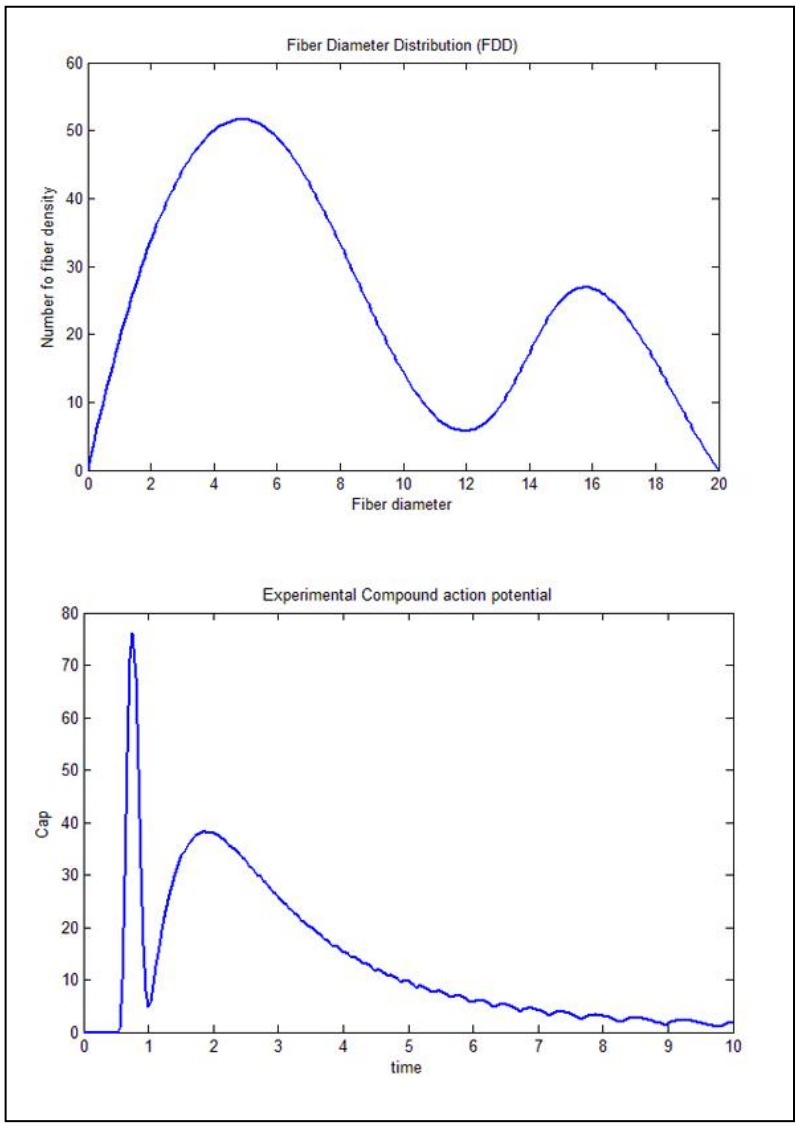

Figure 5.8. Another experimental fiber diameter distribution and compound action potential, respectively.

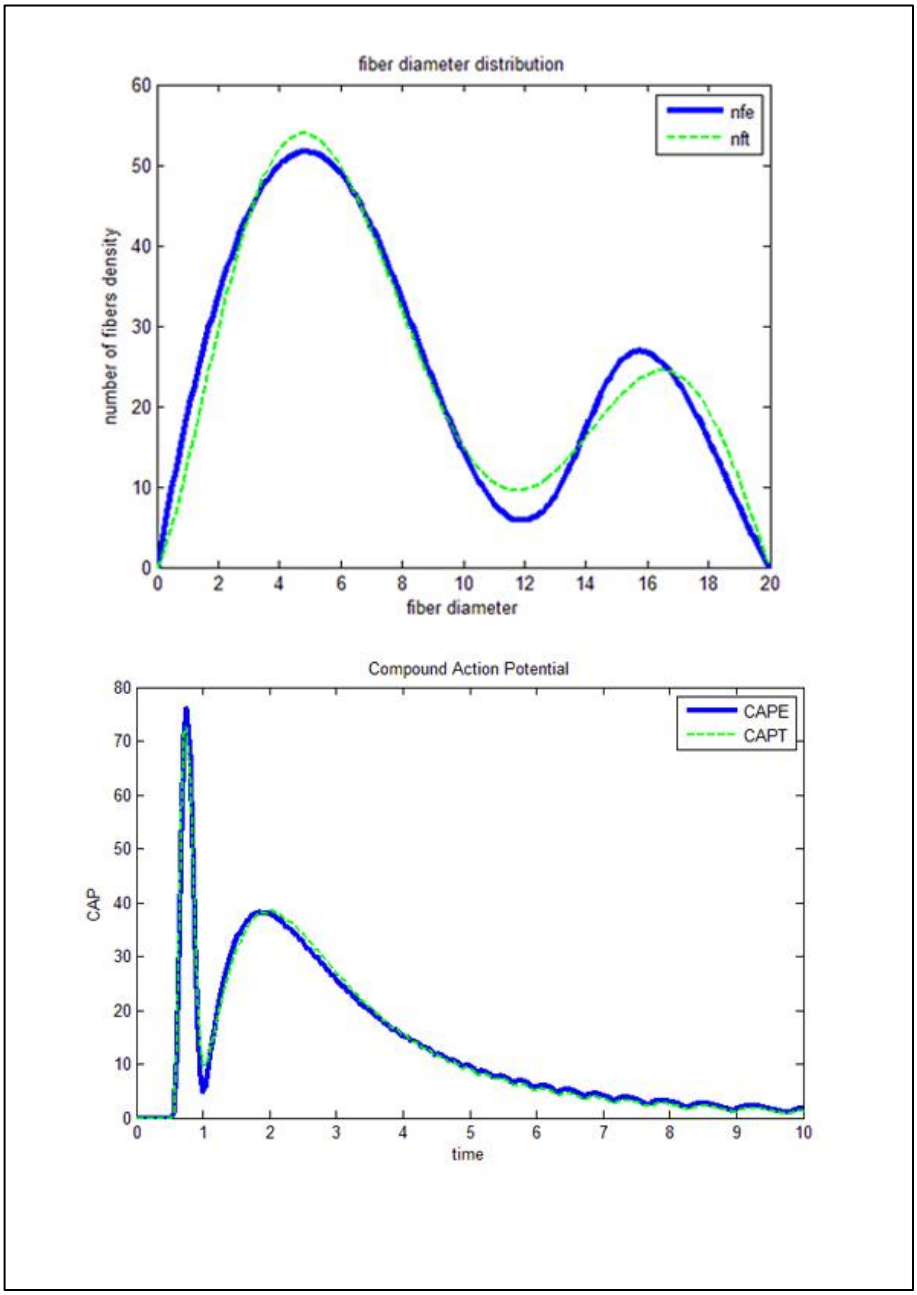

Figure 5.9. Calculated fiber diameter distribution and compound action potential with 6^{th} order polynomial at distance 2 cm.

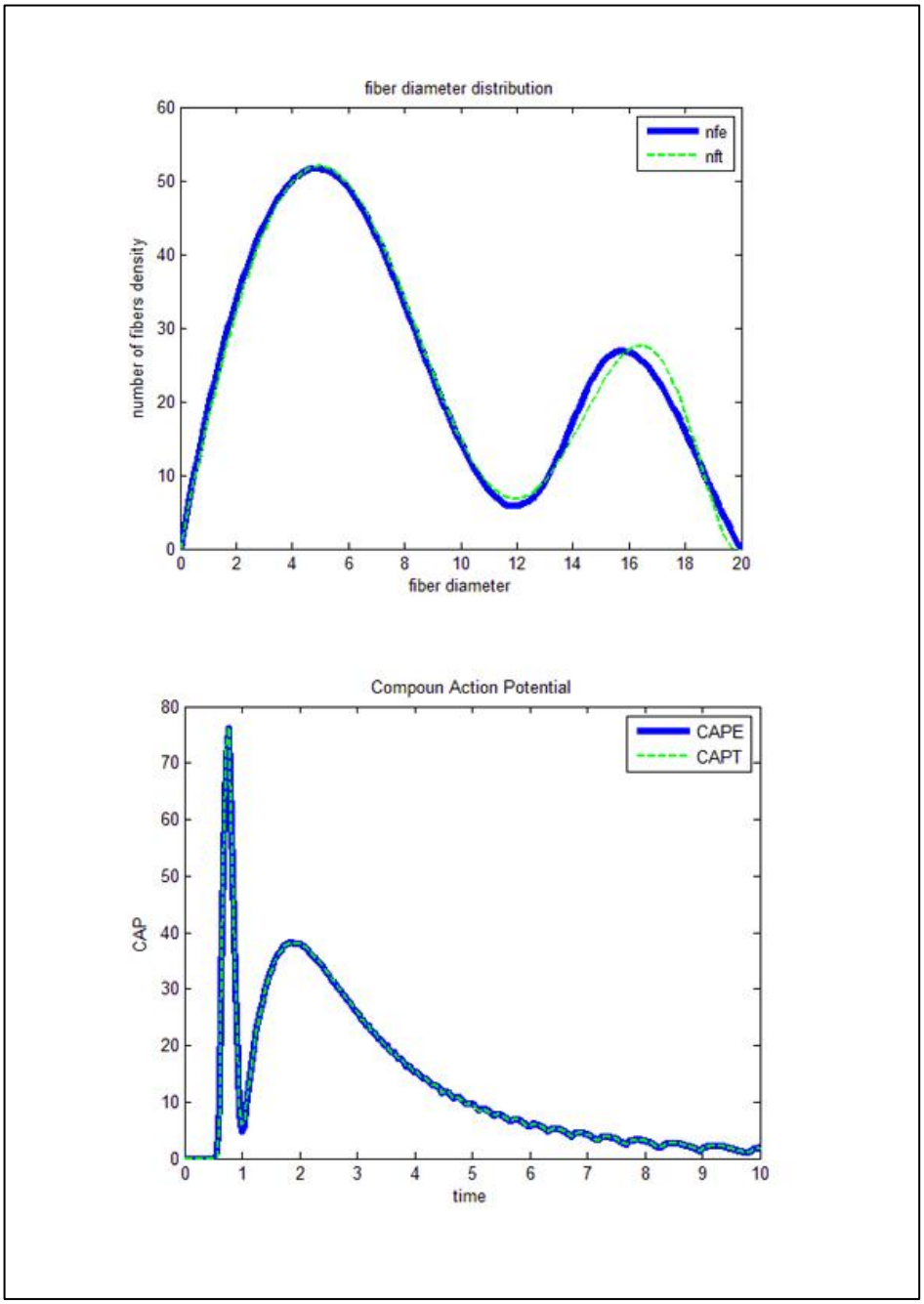

Figure 5.10. Calculated fiber diameter distribution and compound action potential with 8th order polynomial at distance 2 cm.

6. DISCUSSION AND CONCLUSION

In this work, we have developed a continuous approach to the inverse problem of compound action potential (CAP). It involved the determination of a continuous fiber diameter distribution function from a known (such as experimentally measured) CAP data using least-squares optimization. The approach was original since the literature involves only a related discrete approach. In the discrete approach, the fibers are categorized into a predetermined number of groups according to their diameters. The problem leads to an overdetermined system of equations whose solution involves error minimization.

Our approach typically leads to either a small system of linear equations which can be solved directly or a small system of nonlinear equations whose solution is found through Newton-Raphson iteration. . The numerical implementation is relatively straightforward and does not come with a large computational burden.

The presented method seems to perform well in capturing the fiber diameter distribution, especially when using polynomials. One of the main advantages of using polynomials is the fact that it leads to a linear system and always yields a solution. In particular, the distribution based on the 8^{th} order polynomial gives a good fit to fiber distribution of different types and looks robust.

The nonlinear approach, where Gaussian distribution have been utilized worked decently to capture a hypothetical one-peak distribution. On the other hand, we have experienced convergence problems when solving the resulting nonlinear system from a double Gaussian curve. Especially, asymmetric peaks (which are quite common biologically) present in the FDD distribution cannot be captured by the symmetric peaks of the Gaussian distributions. As the actual distribution deviates more from a Gaussian shape, convergence problems becomes more pronounced.

The method utilized in this work is general enough to be implemented with any kind of assumed function with linearly or nonlinearly related parameters. Clearly, the success of this implementation is related with whether the chosen function can simulate actual fiber diameter distributions.

In the literature, CAP and the fiber distribution data expressed simultaneously for a specific nerve seems to be missing in the literature. Hence, we have performed a numerical experimentation in this work where the CAP is generated with the forward problem for realistic fiber diameter distributions available in the literature. The generated CAP is then fed to the inverse problem as if it originates from an experimental measurement where the fiber distribution is unknown.

REFERENCES

Barker, A. T., B. H. Brown, ve I. L. Freeston. «Determination of the distribution of conduction velocites in human nerve trunks.» *IEEE Trans.Biomed.Eng., vol. 26*, 1979: 76-81.

Besr, M. F., B. W. Connors, ve M. A. Paradiso. *Neuroscience Exploring the Brain*. Duckwal Productions., PP.855, 2001.

Brazier, M.AB. *Electrical Activity of the Nervous System.* Pitman Medical Publishing Co Ltd, pp.248, 1977.

Buchthal, F., C. Guld, ve P. Rosenfalck. «Innervation zone and propagation velocity in human muscle.» *Acta Physiol. Scand., vol. 35*, 1956: 174-190.

Caccia, M. R., et al. «Nerve conduction velocity distribution in normal subject and in diabetic patients without neuropathy II. sensory nerve.» *Electromyography and Clinical Neurophysiology,32*, 1992b: 411-416.

Carpenter, R H S. *Neurophysiology.* New York: Co-published in the USA by Oxford University Press, Inc., PP. 308, 1997.

Contento, G., V. Barbinat, M. R. Malisanft, R. Padovanif, R. Budais, ve I. Pittaroli. «Dependence of the linear model for the nerve compound action potential on the single fiber action potential waveform.» *Clin.Phys.physiol.Meas. vol.4, NO.4,*, 1983: 417-433.

Cummins, K. L., D. H. ParkelL, ve L. J. Dorfman. «Nerve fiber conduction velocity distributions. I. estimation based on the single-fiber and compound action potentials.» *Electroenceph. Clin. Neurophysiol., vol. 46*, 1979b: 634-646.

Cummins, K. L., L. J. Dorfman, ve D. H. Parkel. «Nerve fiber conduction velocity distributions.II.estimation based on two compound action potentials.» *Electroenceph Clin. Neurophysiol., vol.46*, 1979a: 647-658.

Dalkilic, N., ve F. Pehlivan. «Comparison of fiber diameter distribution deduced modelling compound action potentials recorded by extracellular and suction techniques.» *International Jurnal of Neuroscience,112*, 2002: 913-30.

Davies, S. W., ve P. A. Parker. «Estimation of myoelectric conduction velocity distribution.» *IEEE Transactions on Biomedical Engineering, vol. 34, NO. 5*, 1987.

Dorfman, L. J. «The distribution of conduction velocities (DCV) in peripheral nerves: a review.» *Muscle Nerve, vol.7, NO. 1*, 1984: 2-11.

Erlanger, J., ve H. S. Gasser. *Electrical signs of Nervous Activity.* Philadelphia: University of philadelphia Press, 1986.

Gasser, H. S., ve J. A. Erlanger. «A study of action currents of nerve with the cathode ray oscillograph.» *Am. J. Physiol., vol. 62*, 1922: 496.

Gonzalez-Cueto, J. A., ve P. A. Parker. «Deconvolution estimation of nerve conduction velocity distribution.» *IEEE Transactions on Biomedical Engineering, vol. 49, NO. 2*, 2002.

Graham, A. J., B. S. Hudgins, ve P. A. Parker. «Polarity correlator for conduction velocity measurement.» *IEEE Trans. Biomed. Eng., vol. 31*, 1984: 675-680.

Gu, D., R. E. Gander, ve E. C. Chrichlow. «Determination of nerve conduction velocity distribution from sampled compound action potential signals.» *IEEE Transactionson Biomedical Engineering, 45(8)*, 1996: 829-838.

Harati, Y. «Diabetic peripheral neuropathies.» *Ann. Intern.Med., vol.107*, 1987: 546-559.

Heinbecker, P., G. H. Bishop, ve J. O'leary. «Pain and touch fibers in peripheral nerves.» *Arch. Neural. Psychiatry, vol. 29*, 1933: 771.

Hirose, G., Y. Tsuchitani, ve J. Huang. «A new method for estimation of nerve conduction velocity distribution in the frequency domain.» *Electroenceph.Clin.Neurophysiol., vol. 63*, 1986: 192-202.

Jasrotia, V. S., ve P. A. Parker. «Matched filters in nerve conduction velocity measurements.» *IEEE Trans. Biomed. Eng., vol. 30*, 1983: 1-9.

Keener, J., ve J. Sneyd. *Mathematical Physiology I: Cellular Physiology.* Springer Science+Business Media, LLC.PP. 470, 2009.

Kiusalaas, J. *Numerical methods in engineering with MATLAB.* Combridge University Press., PP. 431, 2005.

Kovacs, Z. L., T. L. Johnson, ve D. S. Sax. «Estimation of the distribution of conduction velocities in peripheral nerves.» *Comput. Biol.Med., vol. 9, NO. 4*, 1979: 281-293.

Lindstrom, L., ve R. Magnusson. «Interpretation of myoelectric power spectra: A model and its applications.» *Proc. IEEE, vol. 65*, 1977: 653-662.

Lynn, P. A. «Direct on-line estimation of muscle fiber conduction velocity by surface electromyography.» *IEEE Trans. Biomed. Eng., vol. 26*, 1979: 564-571.

Morita, G., X. Y. Tu, Y. Okajima, ve Y. Tomita. «Estimation of the conduction velocity distribution of human sensory nerve fibers.» *Jurnal of Electromyography and Kinesiology,12*, 2001: 37-43.

Papadopoulou, F.A., ve S. M. Panas. «Estimation of the nerve conduction velocity distribution by peeling sampled compound action potentials.» *IEEE Transactions on Magnetics, 35(3)*, 1999: 1801-1804.

Parker, P. A., ve R. N. Scott. «Statistics of the myoelectric signal from monopolar and biopolar electrodes.» *Med. Biol. Eng., vol. 11, NO. 5*, 1973: 491-496.

Paul, D. H. *The Physiology of Nerve Cells.* By Blackwell Scientific Publications Osney Mead, Oxford, England., PP. 114, 1975.

Pollak, V. A., ve Q. X. Wan. «The Z-transform of the compound action potential.» *IEEE Eng. Med.Biol., vol.16, No.3*, 1997: 80-86.

Rubinstein, C. T., ve F. Sharger. «Remyelination of nerve fibers in the transected frog sciatic nerve.» *Brain Research,524*, 1990: 303-312.

Schonhoven, R., ve D. F. Stegeman. «Model and analysis of compound nerve action potentials.» *Critical Reviews in Biomedical Engineering, vol. 19, NO. 1*, 1991: 47-111.

Schoonhoven, R., D. F. Stegeman, V. A. Oosterom, ve G. F. M. Dautzenberg. «The inverse problem in electroneurography-I: Conceptual basis and mathematical formulation.» *IEEE, Trans.Biomed.Eng., vol. 35*, 1988: 769-777.

Seneviratne, K. W., ve O. A. Deiris. «Peripheral nerve function in chronic liver disease.» *J. Neurol.Neurosurg.Psychiat., vol.33*, 1970: 609-609.

Tan, U., ve S. Caliskan. «Modulation of the somatosensory evoked potentials by the input information originating from the gastrocnemius and sural nerves in the dog.» *Int J Neurosci 38(1-2)*, 1988: 151-178.

Tu, X. Y., A. Wernsdorfer, S. Honda, ve Y. Tomita. «Estimation of conduction velocity distribution by regularized-least-squares method.» *IEEE Trans. Biomed. Eng., vol. 44*, 1997: 1102-1106.

Waxman, S. G. «Cellular aspects of conduction in myelinated nerve fibers in relation to clinical deficit.» *Prog Clin Biol Res, VOL. 52*, 1981: 1-15.

Wells, M. D., ve S. N. Gazoni. «A method to improve the estimation of conduction velocity distribution over a short segment of nerve.» *IEEE Transactions on Biomedical Engineering, 46(9)*, 1999: 1107-1120.

Wichman, A., F. Buchthal, C. H. Pezeshkpour, ve A. S. Fauci. «Peripheral neuropathy in hypereosinophilic syndrome.» *Neurology, vol. 35*, 1985: 1140-1145.

CURRICULUM VITAE

I was born in Maragheh, Iran, in 1984. I completed my high school education in Iran and graduated from ERFAN SHAHED high school of Quchan.
I received the B.S degree in Electrical and Electronics Engineering from AZAD University of Birjand, Iran in 2007 then I went to the military service, and finished in 2009. Then I came in Turkey, Adana to continue my education in M.Sc. in 2010.
I have started MSc degree in the department of Electrical and Electronics Engineering in Çukurova University.

My areas of interest include Computer programming, Mathematical modeling of biological systems, biomedical signal and image processing.